CHEMISTRY OF MATERIALS

pubs.acs.org/cm

Article

Carboxyl-Alkyl Functionalized Conjugated Polyelectrolytes for High Performance Organic Electrochemical Transistors

Zeyuan Sun, Brian Khau, Hao Dong, Christopher J. Takacs, Shuhan Yuan, Mengting Sun, Bar Mosevitzky Lis, Dang Nguyen, and Elsa Reichmanis*

Cite This: *Chem. Mater.* 2023, 35, 9299–9312

Read Online

ACCESS | Metrics & More | Article Recommendations | Supporting Information

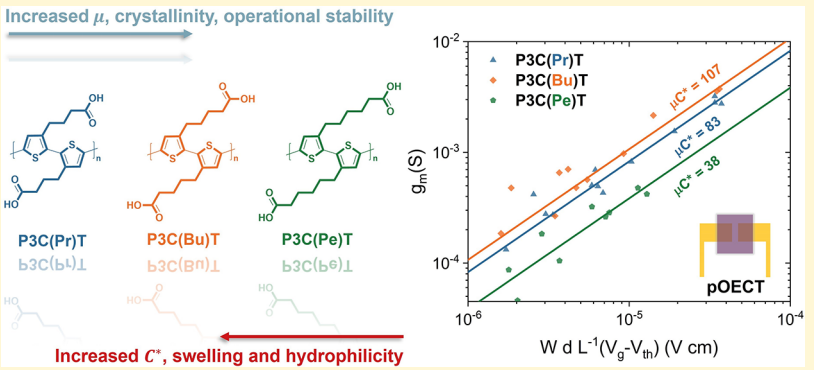

ABSTRACT: Contemporary design principles for organic mixed ionic electronic conductors (OMIECs) are mostly based on the ethylene glycol moiety, which may not be representative of the OMIEC class as a whole. Furthermore, glycolated polymers can be difficult to synthesize and process effectively. As an emerging alternative, we present a series of polythiophenes functionalized with a hybrid carboxyl-alkyl side chain. By variation of the alkyl spacer length, a comprehensive evaluation of both the impact of carboxylic acid functionalization and alkyl spacer length was conducted. COOH-functionalization endows the polymer with preferential intrinsic low-swelling behavior and water processability to yield solvent-resistant conjugated polyelectrolytes while retaining substantial electroactivity in aqueous environments. Advanced in situ techniques, including time-resolved spectroelectrochemistry and Raman spectroscopy, are used to interrogate the materials' microstructure, ionic-electronic coupling, and operational stability in devices. To compare these materials' performance to state-of-the-art technology for the design of OMIECs, we benchmarked the materials and demonstrated significant application potential in both planar and interdigitated organic electrochemical transistors (OECTs). The polythiophene bearing carboxyl-butyl side chains exhibits greater electrochemical performance and faster doping kinetics within the polymer series, with a record-high OECT performance among conjugated polyelectrolytes ($[\mu C^*]_{pOECT}$ = 107 ± 4 F cm^{-1} V^{-1} s^{-1}). The results provide an enhanced understanding of structure−property relationships for conjugated polyelectrolytes operating in aqueous media and expand the materials options for future OMIEC development. Further, this work demonstrates the potential for conjugated polymers bearing alkyl-COOH side chains as a path toward robust OMIEC designs that may facilitate further facile (bio)chemical functionalization for a range of (bio)sensing applications.

INTRODUCTION

Conjugated polymers with the ability to efficiently transport ions and electronic charge are a class of material known as organic mixed ionic-electronic conductors (OMIECs).[1] Owing to the mixed conduction properties, OMIECs promise to serve as central building blocks for a myriad of applications, including battery electrodes,[2−4] supercapacitors,[5,6] electrochromic devices,[7] actuators,[8] and organic bioelectronics.[9−11] In recent years, the latter has seen significant progress because the soft and biocompatible nature of conjugated polymers presents an attractive platform for interacting with living systems. These properties have led to an interest in developing active materials for low-voltage bioelectrochemical devices, such as organic electronic ion pumps,[12] neuromorphic modules,[13] electrophysiological monitoring,[14] and organic electrochemical transistors (OECTs).[15] Owing to the high-fidelity transduction of biological signals into electrical output, OECTs are emerging as a "mainstay" contemporary sensing platform.[15] Conventional OECTs have a three-terminal device

Received: August 18, 2023
Revised: October 10, 2023
Accepted: October 18, 2023
Published: November 2, 2023

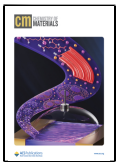

architecture akin to that of organic field effect transistors (OFETs), comprising a source, drain, and gate electrode as well as an active polymer thin film that serves as the channel bridging the source and drain regions. OECTs diverge from solid-state OFETs in that they utilize an electrolyte interface instead of a dielectric layer between the gate and channel regions. Operatively, the working principles of OECTs hinge upon the use of the OMIECs, which possess distinct properties to enable dual conduction pathways for ions/water and ionic-electronic coupling. In this aspect, OECTs exhibit many advantages as ideal devices for both sensing and amplifying biological signals at low operating voltages with high transconductance in a wearable motif.[16]

As OECTs continue to improve, exploring diverse material platforms becomes vital for further innovation. Contemporary OMIEC design approaches capitalize on high electron/hole mobility backbones where their alkyl side chains have been replaced with alternative polar moieties to facilitate ion transport.[17] The most widely utilized and studied OMIEC is the commercially available poly(3,4-ethylenedioxythiophene)/poly(styrensulfonate) (PEDOT/PSS), where electronic conduction takes place along the conjugated backbone of PEDOT, and the negatively charged sulfonate groups on PSS provide more ion-accessible sites for efficient ionic conduction.[18,19] The relatively low power efficiency of the depletion operational mode,[20] the limitation of volumetric capacitance owing to the insulating PSS phase,[21] and the added requirements of cross-linker along with intricate preparatory and subsequent postdeposition processing[22,23] make PEDOT/PSS a complex and nonideal material for OMIEC study and integration into biological applications.

The predominant approach for generating OMIEC materials revolves around side chain engineering of nonionic polar substituents incorporated onto known conjugated (semi)-conducting polymer backbones.[17,24] Specifically, the incorporation of oligo(ethylene glycol) (OEG) side chain motifs have garnered significant attention; this motif has yielded an extensive array of high-performance OMIEC materials using conjugated backbones such as poly(propylenedioxy-thiophene) (PProDOT),[25] polythiophene,[26] bithiophene-thienothiophene,[27] and naphthalene diimide-bithiophene (NDI-T2).[28] OEG functionalization enables facile ion uptake and swelling via hydrogen bonding with the aqueous environment,[29] leading to enhanced volumetric capacitance (C^*) and improved device transconductance (g_m).[26−28] Yet OEG side chains, and similar, present significant synthetic and purification challenges.[30] The hydrophilic nature often increases sensitivity to environmental factors such as humidity and temperature,[31] as well as reduced solubility in organic and aqueous solvents.[32] Furthermore, endowing polymers with OEG side chains may induce structural irregularities (backbone twist/torsion) and undesired swelling upon electrochemical doping, thereby significantly restricting electron/hole transport (μ) and reducing long-term stability.[33] While several promising OMIEC materials bearing OEG side chains have been developed, they exhibit limitations that restrict rapid iteration in the materials space. As a result of these factors, systematic development of structure−property relationships governing the performance of the OMIEC has proved challenging.

To address the aforementioned issues, one emerging strategy introduces hydrophobic alkyl spacers between the conjugated backbone and the hydrophilic side chain to form amphipathic side chains. Substituting a full-length OEG side chain with a short methyl or ethyl spacer presents a viable approach to enhance polymer crystallinity and improve volumetric capacitance.[29] Similar studies with longer alkyl group spacers were also conducted in a series of mixed conduction donor−acceptor (D−A) copolymers,[34−36] where controllable swelling and charge transport with improved processability and stability was demonstrated. These studies highlight the significant potential in enhancing the overall functionality and reliability of the OECTs through the manipulation of molecular structures through side chain engineering.

Prevailing OMIEC design principles, however, rely heavily on the ethylene glycol moiety, limiting the ability to tailor the OMIEC chemistry to serve the vast application space for OECTs. To create transformational opportunities for future OMIEC materials, additional structural alternatives must be considered and explored. One design strategy, which integrates covalently attached pendant ionic side chains to yield a conjugated polyelectrolyte (CPE), was recently introduced as a promising OMIEC alternative.[17] The polar electrolyte groups impart enhanced ion mobility and versatile processability. Examples of CPEs that were successfully integrated into OECT applications include sulfonate bearing polythiophenes,[18,37] polyethylenedioxythiophenes,[38] and their blends.[39] More recently, a self-doped ambipolar conjugated polyelectrolyte with dual operation mode, poly[2,6-(4,4-bis-potassium butanylsulfonate-4*H*-cyclopenta-[2,1-*b*; 3,4-*b*′]-dithiophene)-*alt*-4,7-(2,1,3-benzothiadiazole)] (CPE-K) has also been reported.[40] However, the intrinsic water solubility can lead to severe degradation during device operation, and adding a cross-linker will sacrifice mixed conduction and overall performance. Hence, a significant knowledge gap in the OECT field lies in the absence of high-performance polymer systems that are both additive-free and highly processable.

Previously, we demonstrated a high performance carboxylated polythiophene, poly [3-(4-carboxypropyl) thiophene] (P3C(Pr)T), as a promising alternative candidate toward a reliable mixed conducting structure.[41] With a facile post-acidification step, the aqueous-compatible carboxylated salt precursor was transformed into a solvent-resistant carboxylic acid functionalized polythiophene obviating the use of cross-linkers. In addition, the acidifying agent (*p*-toluenesulfonic acid) does not subsequently remain in the postprocessed film. The carboxylic acid-functionalized product exhibited robust processability, promising electrochemical properties (e.g., fast redox kinetics, competitive volumetric capacitance) and OECT potential.[41] In addition, the COOH-functionalized materials offer a plethora of appealing features, including synthetic accessibility and opportunities for further chemical transformation. More importantly, the −COOH moiety exhibits low intrinsic cytotoxicity with exceptional biocompatibility[42] and offers opportunities to create hydrogel matrices and covalently bind biological molecules (e.g., peptide attachment),[43] which demonstrate a broader range of postfunctionalization opportunities for biomedical and biosensing applications, such as electroconductive 3D scaffolds and aptamer-based sensing.[42,44,45] To date, however, the existing library of OMIEC materials lacks comprehensive study of carboxylic acid-substituted conjugated polymers: neither the functionality of the ionic carboxylated side chain motif nor the impact of alkyl spacer lengths in conjugated polyelectrolytes have been

https://doi.org/10.1021/acs.chemmater.3c02103
Chem. Mater. 2023, 35, 9299−9312

investigated, severely limiting the synthetic toolbox for future OMIEC development.

With these considerations in mind, we investigated a family of carboxylic acid functionalized polythiophenes possessing a hybrid alkyl-ionic side chain moiety. A systematic study of the acid functionalized propyl (C_3) derivative compared to polythiophenes bearing either a butyl (C_4) or pentyl (C_5) spacer was conducted. With the aid of a fully aqueous processing strategy, this series of materials provides a framework for evaluating the effect of the alkyl spacer length and the impact of the carboxylic acid functionality on the polymers' electrochemical characteristics in aqueous electrolytes. Additionally, in situ Raman and spectroelectrochemistry studies provide meaningful insights into structural reorganization and optical progression upon electrochemical doping/dedoping, yielding a molecular level understanding toward ionic-electronic coupling. Quartz crystal microbalance with dissipation monitoring (QCM-D) measurements were also performed to elucidate the controllable volumetric changes associated with the hybrid side chain functionality. Furthermore, integration of these high-performance mixed conductors into both interdigitated and planar OECT architectures facilitated the evaluation of material dependent properties, including device performance and stability as well as geometry-dependent effects. Through these investigations, we uncovered distinct functionalities and properties that provide a more comprehensive picture of relevant structure and property relationships for these high-performance conjugated polyelectrolytes.

EXPERIMENTAL SECTION

Materials. P3KBuT (poly(3-(potassium-4-butanoate) thiophene-2,5-diyl), M_w = 21 kDa, PDI = 2.2, RR = 89%); P3KPeT (poly(3-potassium-5-pentanoate) thiophene-2,5-diyl), M_w = 28 kDa, PDI = 2.0, RR = 89%); P3KHeT (poly(3-potassium-6-hexanoate) thiophene-2,5-diyl), M_w = 35 kDa, PDI = 2.4, RR = 86%); and P3HT (poly(3-hexylthiophene-2,5-diyl), M_w = 74 kDa, PDI = 2.2, RR = 96%) were purchased from Rieke Metals Inc. *p*-Toluenesulfonic acid monohydrate (*p*TsOH-H_2O, 98%, Sigma-Aldrich), sodium chloride (99.9%, biotechnology grade, VWR), acetone (99.5%, Sigma-Aldrich), methanol (99.8%, Sigma-Aldrich), and isopropyl alcohol (99.5%, Sigma-Aldrich) were used as received. Deionized (DI) water with a resistivity of 18.2 mΩ cm was obtained using an Aries water purification system (ARS-105).

Film Preparation, Electrochemical, Optical, and Transistor Measurement. *Film Preparation.* The conjugated polymer thin films were fabricated following the previously reported method.[41] In brief, conjugated polyelectrolyte precursor solutions were prepared in water at a concentration of 2 mg mL^{-1} and stirred at room temperature overnight. The resulting polymer solution was then spray-cast (Iwata Eclipse HP-CS airbrush, gravity feed) onto glass/ITO/OECT device substrates heated to 80 °C. The thin films were then transformed into solvent-resistant acid form through immersion into 0.1 M *p*TsOH-H_2O in methanol for 5−10 min, successively rinsing with methanol and water, and blow drying under nitrogen prior to measurement.

Cyclic Voltammetry. (CV) was conducted by using a Gamry Reference 3000 Potentiostat/Galvanostat and a three-electrode setup. The working electrode (WE) was prepared by spray-coating the conjugated polymer films from their respective potassium salt precursors onto ITO-coated glass slides (Delta Technologies, resistivity = 8−12 Ω sq^{-1}), which were then acidified to yield P3CATs. A stainless-steel plate was used as the counter electrode (CE), and a standard Ag/AgCl electrode (3 M aqueous NaCl inner solution, BASi) was used as the reference electrode (RE). 0.1 M NaCl (aq) solution was used as the electrolyte. To ensure accurate measurements, all electrolytes were degassed under argon flow for 15 min both prior to and during the measurement process. The scans were recorded at a scan rate of 50 mV s^{-1} with a step size of 2 mV.

In Situ Spectroelectrochemical. In situ spectroelectrochemical measurements were performed by using the same setup as in CV with a three-electrode configuration in a 0.1 M NaCl aqueous solution under a nitrogen atmosphere. The WE and RE were the same, and a platinum flag was used as the counter electrode (CE). The experiment was conducted using an Agilent Cary 5000 spectrophotometer with quartz cuvettes with a path length of 1 cm. Before recording the spectra, the carboxylated polythiophene film was electrochemically conditioned, involving 20 cycles of CV scans in the range of −0.5 to +1 V vs Ag/AgCl, with a scan rate of 50 mV s^{-1}. The purpose of conditioning was to ensure reproducibility of the redox characteristics of the polymer. Following the conditioning process, the film was biased under potentiostatic conditions, incrementing the potential in steps of 100 mV, starting from the most cathodic potential and biasing toward more anodic conditions. The film spectra were recorded once WE current reached a steady state which typically required 30 to 60 s for each 100 mV step.

Electrochemical Impedance Spectroscopy. EIS was conducted by using the aforementioned three-electrode setup. The measurement involved applying a 10 mV amplitude scan between 0.1 Hz to 100 kHz. The WE were initially conditioned at the probed DC voltage for 60 s to ensure a steady-state condition. This step was performed to establish the in-film doping level before the 10 mV AC perturbation was applied.

Atomic Force Microscopy. AFM measurements were performed on a Bruker Dimension Icon by MSE Supplies LLC to measure the thickness of the spray-cast thin film on a silicon/glass substrate for each polymer. An average 10 × 10 μm section was taken to provide an accurate measurement across the samples. An excitation frequency of 80 kHz was used, with a scan rate of 0.8 Hz. Height images were recorded and then processed through NanoScope Analysis software.

OECT Fabrication and Characterization. Interdigitated organic electrochemical transistors (iOECTs) were purchased from MicruX technologies (Model ED-IDE1-Au, total area = 38.5 mm^2, 10 μm electrode length, 10 μm electrode gap, gold thickness = 150 nm, active area = 9.6 mm^2, average width = 2.75 mm). The as-prepared potassium salt polymer solutions (P3KATs) were spray-cast onto iOECT substrates and subsequently acidified as noted to yield P3CAT thin films. The resulting polymer thickness ranged from 80 to 300 nm. Planar organic electrochemical transistors (pOECTs) were designed in-house and fabricated through Platypus Technologies, LLC. In summary, small channel devices (W = 100 μm, L = 50, 100, 200, 400 μm) and large channel devices (W = 1000 μm, L = 100, 200 μm) were patterned by vapor-deposition of titanium (10 nm), followed by gold (100 nm) through a photomask onto cleaned glass substrates. The titanium layer was integrated to allow better adhesion of gold to the glass substrate. A negative photoresist (SU-8) was then photolithographically patterned on top of the aforementioned metal to insulate against contact by an aqueous electrolyte. A customized stencil mask was laid on top of the channel area, followed by potassium salt (P3KAT) polymer spray-casting and acidification to complete the P3CAT deposition process. A cylinder-shaped Ag/AgCl pellet (Warner Instruments) was used as a gate electrode and immersed in a 0.1 M aqueous NaCl solution confined in a PDMS well. Transfer and output characteristics were measured with an Agilent B1500A semiconductor analyzer. All transistor characteristics were collected by using Keysight Easy Expert software with a custom I/V sweep configuration and were tested under ambient conditions. Data were collected for at least five separate devices to ensure reproducibility. Output curves were collected with a V_d step size −0.1 mV, and a V_g step size of −0.1 V. Transfer curves were collected using a V_d = −0.6 V with a V_g step size of −0.1 mV. Stability tests were collected using a V_d = −0.6 V, and a V_g step of −1 mV for 500 cycles. The data were further analyzed through RStudio Version 1.2.1335 to extract the transconductance (g_m) and peak drain current.

Swelling Analysis. Passive swelling measurements were conducted with a QSense Explorer Analyzer (Biolin Scientific AB, Sweden).

https://doi.org/10.1021/acs.chemmater.3c02103
Chem. Mater. 2023, 35, 9299−9312

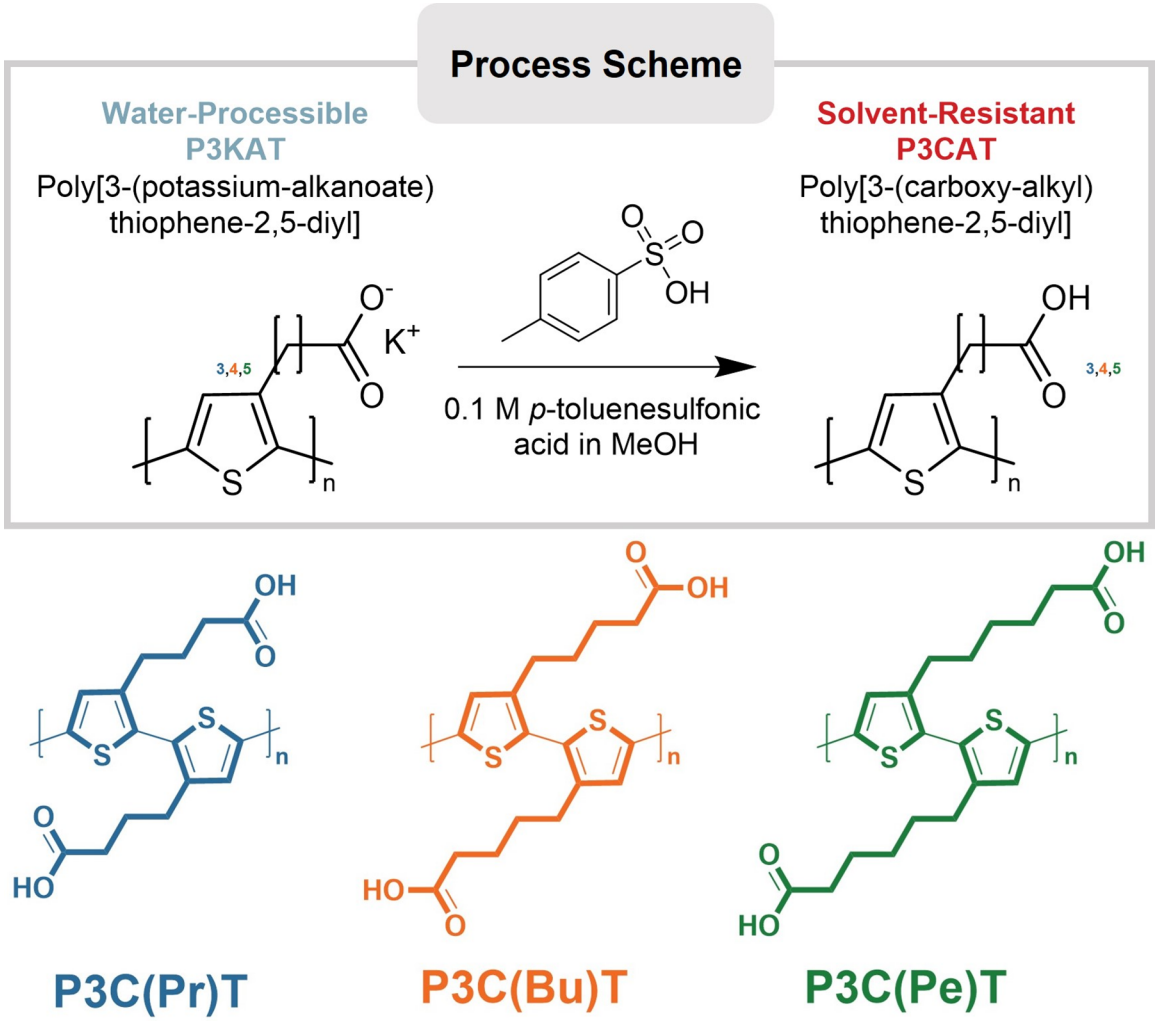

Figure 1. Schematic representation of the generalized acidification step of water-soluble poly[3-(potassium-alkanoate)thiophene-2,5-diyl] (P3KAT) to form solvent resistant poly[3-(carboxyl-alkyl)thiophene-2,5-diyl] (P3CAT) (top) and the chemical structures of the carboxyl-alkyl side chain polythiophenes studied here (bottom). The same color scheme, namely P3C(Pr)T (blue), P3C(Bu)T (orange) and P3C(Pe)T (green) is used throughout.

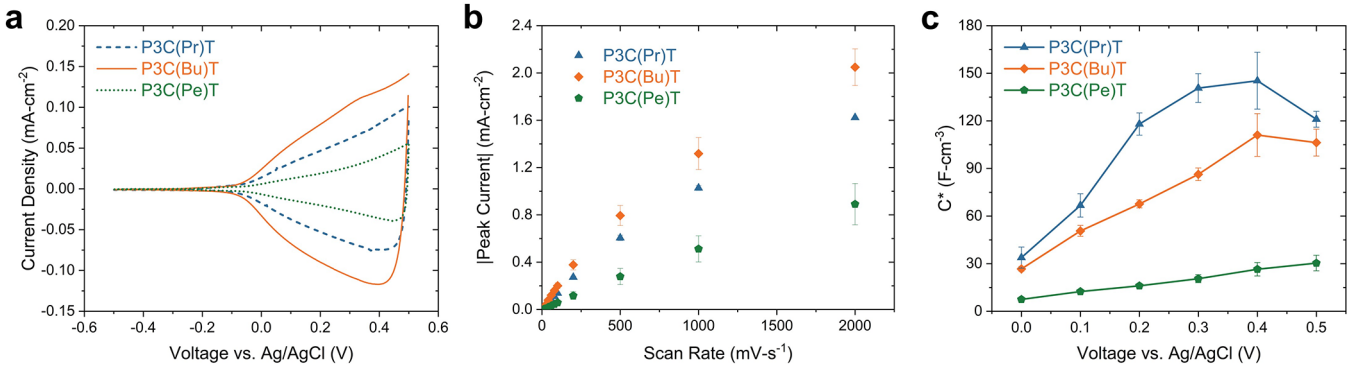

Figure 2. (a) Cyclic voltammetry (CV) with a rate of 50 mV s^{-1}. (b) Peak current density as a function of scan rate. (c) Volumetric capacitance determined by electrochemical impedance spectroscopy for P3C(Pr)T (blue triangle), P3C(Bu)T (orange diamond), and P3C(Pe)T (green pentagon).

First, the response of the bare Ti/Au sensors were recorded using QCM-D in air conditions, followed by measurements after injection of 0.1 M NaCl (aq) electrolyte into the chamber. These control measurements resulted in significant shifts in frequency and dissipation due to density differences between the media, which were excluded from the swelling percentage calculation. The sensors were then removed, and the conjugated polymer films were spray coated directly onto the same sensors, followed by acidification steps as mentioned above. The absolute difference in frequency between the bare sensor and the Ti/Au/polymer coated sensors was compared using the "stitched data" function of Q-Soft software. This function accounted for density differences and allowed for the direct

https://doi.org/10.1021/acs.chemmater.3c02103
Chem. Mater. 2023, 35, 9299−9312

determination of mass changes per unit area using the Sauerbrey equation (eq 1). The calculated mass changes were then converted to thickness changes, considering the sensor area and assuming a density of 1 g cm^{-3} for the polymers in different states (dry and wet).

$$\frac{\Delta m}{A} = \frac{-17.7}{n}\Delta f_n \quad (1)$$

Raman Spectroscopy. Raman spectra were obtained using a Horiba LabRAM Odyssey confocal Raman microscope with a 633 nm excitation laser source in a backscattering geometry. The spectra of the dry films were measured though a 50× objective, while the spectra of films exposed to the electrolyte were measured using a 5× objective. The laser power was set at 50% power (8.5 mW) for all conditions to avoid photothermal effects and sample degradation. For all measurements, thin films of target polymers were spray cast onto ITO/glass substrates (8−12 Ω sq^{-1} Delta Technologies), then acidified as per above and used as working electrodes. Ag/AgCl pellet (D = 2 mm × H = 2 mm, Warner Instruments) and Pt wire were used as RE and CE, respectively. A Gamry interface 1000 Potentiostat was used to perform in situ doping and dedoping experiments. All measurements were taken in an AIST-NT EC001 electrochemical cell filled with a 0.1 M NaCl (aq) electrolyte. The spectral region scanned in this investigation ranged between 600 and 1799 cm^{-1}. A silicon wafer was used for the calibration process, and all spectra were collected using LabSpec 6 software and further deconvoluted through PeakFit version 4.12 software.

RESULTS AND DISCUSSION

Aqueous Electrochemical Characterization. Water solutions (2 mg mL^{-1}) of P3K(Bu)T, P3K(Pe)T P3K(He)T were spray cast onto ITO/glass surfaces and subsequently acidified in a 0.1 M *para*-toluenesulfonic acid/methanol solution to produce the solvent-resistant carboxyl-alkyl polythiophene derivatives, namely, P3C(Pr)T, P3C(Bu)T, P3C(Pe)T. The detailed process scheme is shown in Figure 1.

Cyclic voltammetry (Figure 2a) was used for preliminary evaluation of the electrochemical characteristics of P3C(Pr)T, P3C(Bu)T, and P3C(Pe)T films over the course of 5 charge/discharge cycles using 0.1 M aqueous NaCl as the electrolyte. At 50 mV s^{-1}, the carboxylated polythiophenes undergo repeated oxidization and reduction within the electrochemical stability range and exhibit evidence of unipolar p-channel doping, as indicated by the emergence of a broad oxidation onset above −0.2 V. To prevent potential degradation caused by either excessive polymer oxidation or side reactions related to breakdown of water, the polymers were not oxidized beyond 0.5 V vs Ag/AgCl. Notable differences in both current density and onset potential were observed across the series (Figure 2a); of the three systems, P3C(Bu)T exhibited the lowest onset potential at −0.3 V and the highest peak current density. Varying the alkyl spacer length relative to the butyl alternative led to a shift toward higher onset potential and lower current density, with the propyl analogue exhibiting an onset of −0.06 V, and the pentyl derivative showing an onset potential of −0.23 V. To eliminate the possible influence of background currents, differential pulse voltammetry (DPV) was conducted to validate the oxidation onset as shown in Figure S1. A comparable pattern of onset potential was observed, with the polymer bearing propyl, butyl, and pentyl spacers showing values of −0.11, −0.17, and −0.15 V, respectively. These findings align with CV analysis where P3C(Bu)T exhibits an earlier onset potential and better electrochemical response than the two alternatives. Despite achieving a lower current density, P3C(Pe)T exhibited a reduced onset potential relative to P3C(Pr)T in both CV and DPV tests. This result suggests that the longer alkyl spacer is more easily oxidized in contact with the electrolyte, resulting in faster ion migration and response.[46]

To evaluate the kinetics of the redox processes, the dependence of the peak current density on the scan rate (ν) was investigated using CV (Figure 2b). By assuming negligible charge transfer resistance between the polymer film and the electrode and considering the films to be uniform and thin, this analysis provided insight into identifying critical scan rate, where mass transport limitations started to dominate, associated with ion migration (doping/dedoping process).[47,48] As presented in Figures 2b, S2 and S3, all three polythiophenes exhibited relatively linear dependencies of the peak current close to 500 mV s^{-1}, indicating favorable charge and discharge kinetics for future biological applications. Notably, the polymer with the longest alkyl side chain, P3C(Pe)T, exhibited linear dependency in both the low and high scan rate regions up to 1000 mV s^{-1}, and the largest critical scan rate prior to mass transfer limitations. However, significantly lower current densities can be observed in P3C(Pe)T compared with the other two polymers, especially at higher scan regions. Most likely, the longer alkyl chain reduced the ability of P3C(Pe)T to store an electronic charge. Further, the pentyl spacer likely renders the polymer more rigid and hydrophobic compared to its shorter alkyl chain counterparts, hindering penetration of ions, thus leading to limited access of ion-electron coupling or even repulsive interactions.[32,49] Additionally, side chain induced conformational changes may also play a role in preventing a high charge density along the conjugated backbone. The log−log plot of current density vs scan rate was created to precisely identify the transition of the diffusion-limited regime. As shown in Figure S2 and Table S1, in contrast to the initial qualitative observation, the linear regime is only present within a time window spanning one to 2 orders of magnitude with approximate thresholds for mass transfer limited regime at ∼400 mV s^{-1}, and a superlinear regime emerging at extremely low scan rates up to 50 mV s^{-1}. Thus, for biological applications, 400 mV s^{-1} is more than sufficient for most envisioned applications, and diffusion and mass transfer are not limited to the scan rate used in CV.

The charge storage capability of the carboxylic acid substituted polythiophenes was investigated using EIS. The volumetric capacitance, C^*, is a crucial parameter needed to evaluate and compare the steady-state capacitive behavior of channel materials used in OECTs.[21] Given that conjugated polymer/polyelectrolyte blend systems, such as PEDOT/PSS, may deviate from the ideal capacitive charging approximation,[50,51] a diffusion-modified Randles circuit model was employed. This model accurately deconvolutes the overall capacitance into two distinct contributions, a non-Faradaic component attributed to the double-layer effect and a Faradaic component associated with pseudocapacitance.[41,52] The circuit configuration is presented in Figure S4; the electrolyte resistance (R_e) is interconnected with a parallel arrangement of double-layer capacitance (C_{DL}), while a series combination of the charge-transfer resistance (R_{CT}), a Warburg element, and the pseudocapacitance (C^*) follows. The impedance data were fit to the circuit to obtain the capacitance, then normalized by film volume to determine the volumetric capacitance. The volumetric capacitance decreases from 145 ± 18, 111 ± 14, and 30 ± 5 F cm^{-3} for P3C(Pr)T, P3C(Bu)T and P3C(Pe)T, respectively(Figure 2c). This finding demonstrated a trend wherein the increase in alkyl spacer length led

https://doi.org/10.1021/acs.chemmater.3c02103
Chem. Mater. 2023, 35, 9299−9312

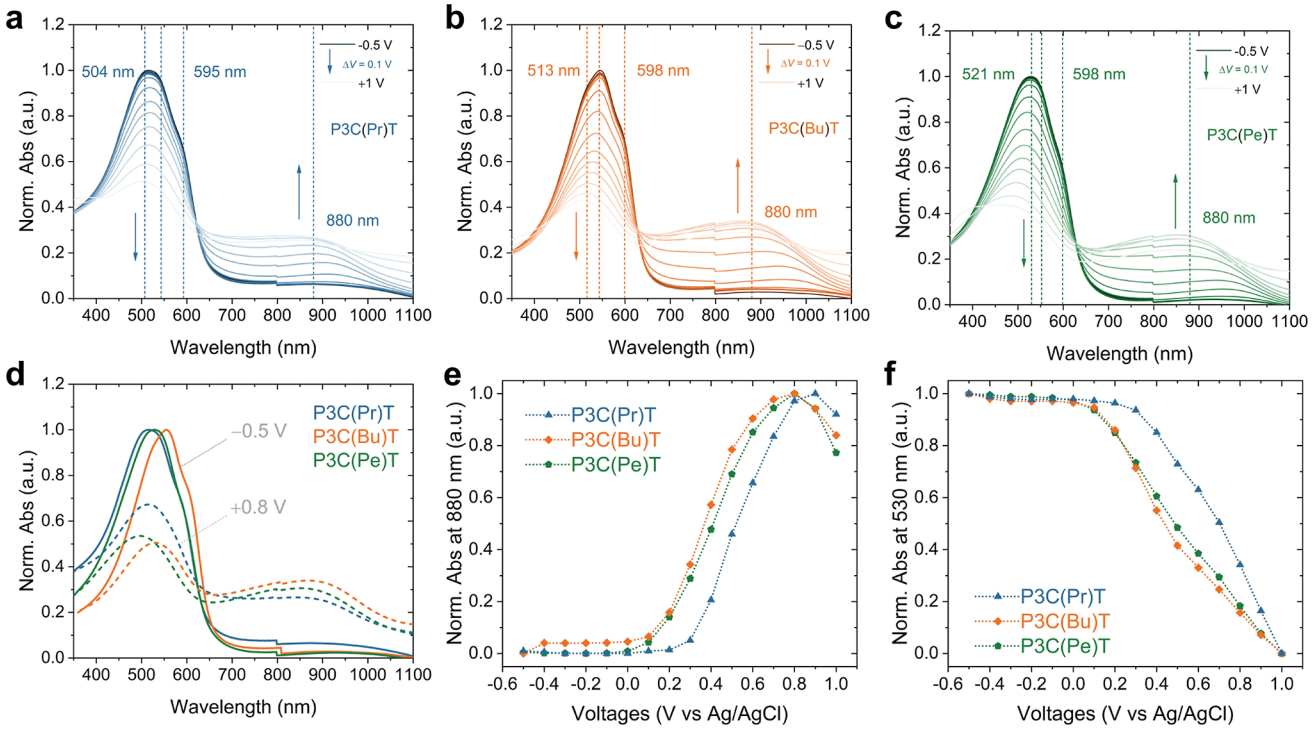

Figure 3. Spectroelectrochemistry of (a) P3C(Pr)T, (b) P3C(Bu)T, and (c) P3C(Pe)T spray-cast film biased at −0.5 to 1 V versus Ag/AgCl in degassed 0.1 M NaCl (aq). (d) Superimposed UV−vis−NIR absorbance spectra of spray cast P3C(Pr)T (blue), P3C(Bu)T (orange), and P3C(Pe)T (green) at −0.5 V (dedoped, solid line) and +0.8 V (doped, dashed lines) vs Ag/AgCl in 0.1 M NaCl (aq). (e,f) Evolution of steady state absorbance upon electrochemical doping from −0.5 to 1 V at (e) polaron formation peak at 880 nm and (f) 0−1 peak at 530 nm.

to a dramatic reduction of volumetric capacitance. The observed pattern is comparable to results of several studies exploring the impact of alkylated content on the side chain where C^* was shown to be dependent upon both the extent of active material swelling and hydrophilicity.[34,53,54] Hence, striking a fine balance in alkyl moiety chain length is crucial to optimize the capacitive response in the design of −COOH functionalized conjugated polymers. While minor increases proved to be beneficial, an excessive alkyl content will likely incur detrimental effects.

To further investigate the apparent correlation between alkyl spacer length and volumetric capacitance, quartz crystal microbalance with dissipation monitoring (QCM-D) studies were conducted to assess the swelling behavior of the carboxylated polythiophenes upon exposure to electrolyte. In agreement with previous findings and consistent with contact angle measurements (Figure S6),[34,54] the largest degree of passive swelling was observed for the polymer with the shortest alkyl spacer (P3C(Pr)T, ≈17.9%); while P3C(Bu)T and P3C(Pe)T displayed progressively lower levels, namely ≈12.3% and ≈2.5%, respectively (Figure S5 and Table S2). The results indicate that the thin-film hydrophobic character is enhanced as alkyl chain length increases, although the potential effect of molecular weight on these systems cannot be eliminated. Remarkably, while P3C(Pe)T displayed a comparable surface hydrophilicity to PEDOT/PSS (water contact angle ≈ 63°),[30] the pentyl polythiophene derivative featured a significantly lower degree of passive swelling (2.5% vs 85% for PEDOT/PSS).[55] This finding suggests that carboxylated polythiophenes are characterized by a lower level of bulk hydrophilicity reflected in the dramatic swelling difference. Such a hydrophobic nature could potentially aid in preserving ordered structure, positively affecting hole/electron conduction and ion migration. These attractive features for carboxyl-alkyl functionalization remain compelling in comparison to other classes of conjugated polymer OMIECs. For example, poly[3,3′-bis(2-(2-(2-methoxyethoxy)ethoxy)ethoxy)-2,2′-bithiophene] (p(g3T2)), with an equivalent number of side chain carbons as P3C(Pe)T undergoes a volumetric change of 50%;[56] while comparing P3C(Bu)T to poly(2-(3,3-bis(2-(2-(2-methoxyethoxy)ethoxy) ethoxy)-[2,20-bithiophen]-5-yl)-thieno[3,2-*b*]thiophene) (p(g2T-TT)), both polymers exhibit similar degrees of passive swelling (≈10%). It is noteworthy that −COOH functionalization provides for similarly low levels of swelling as recently reported high-performance OMIECs, but with a lower proportion of hydrophobic content.[57] A reduction in swelling was also reported for conjugated polyelectrolyte copolymers, such as poly[6-(thiophen-3-yl)hexane-1-sulfonate tetramethylammonium]-*co*-poly(3-hexyl thiophene) (PTHS$^-$TMA$^+$-*co*-P3HT), however the copolymer design introduces synthetic complexity and OECT performance is significantly reduced due to the introduction of the 3-hexylthiophene units.[37] A detailed list of OMIEC polymer candidates and associated swelling is provided in Table S3 in the Supporting Information.

The observed significant decrease in passive swelling from 18% to 2% for P3C(Pr)T and P3C(Pe)T, respectively, is both promising and potentially useful. P3C(Pr)T exhibits the highest degree of passive swelling of this series, yet undergoes substantially less passive swelling than OMIECs bearing ethylene glycol or alternative pendant ionic moieties that frequently experience unwanted volumetric expansion and plasticization.[26,57] From an operational perspective, repeated swelling/deswelling may compromise mechanical integrity with reduced volumetric capacitance,[58] resulting in active layer delamination and reduced device lifetime. These factors

https://doi.org/10.1021/acs.chemmater.3c02103
Chem. Mater. 2023, 35, 9299−9312

underscore the importance of reducing swelling-induced effects during device operation and highlight the favorable intrinsic characteristics imparted by −COOH functionalization for low-swelling OMIEC designs.

Moreover, with a controlled fraction of alkyl content, the carboxylated side chain alternative allows modification of polymer bulk hydrophilicity with tunable swelling, which can further fine-tune ion migration and mixed conductivity.[59,60] Within the P3CAT series, the increased bulk hydrophilicity of P3C(Pr)T may lead to excess swelling during electrochemical doping−dedoping, with a concomitant decrease in electron/hole transport. Together, these factors lead to diminished electronic response as evidenced by the observed low onset potential and moderate current density (Figure 2a,b). In contrast, the longer alkyl spacer alternatives, such as P3C(Pe)T, restrict the extent of swelling, hindering ion penetration into the bulk due to fewer sites for electrolyte−polymer interaction, and thus decreasing current density.[53] The alkyl spacer in P3C(Bu)T provided a balance that ensures optimal ion penetration and storage capabilities while exhibiting the ability to carry the highest amount of charge during electrochemical cycling in comparison to its analogues. Consequently, to achieve optimal charging capabilities, tuning the hydrophilicity through side chain engineering is paramount in the design of −COOH functionalized conjugated polymers for OECT applications. The electrochemical results combined with the swelling analysis provide compelling evidence that the incorporation of carboxyl-alkyl side chains represents a promising and effective strategy for precisely manipulating the extent of swelling and mixed conduction in polymer films.

In Situ Structural and Photophysical Analysis. Changes in the carboxylated polythiophene photophysical characteristics, doping mechanism, and oxidation behavior were investigated using in situ spectroelectrochemistry. Figures 3a−c and S7 present the normalized and non-normalized evolution of the absorption spectra as a function of potential in the range of −0.5 to 1 V, in increments of 0.1 V. All three polymers exhibited a decrease in features associated with the neutral state in the range of 500−600 nm (2.0−2.8 eV), with concomitant increase in a charged feature in the near-IR (∼800 to 1100 nm) indicating polaron formation. As cast, the polythiophenes appear to demonstrate H-like aggregation, with a less intense lower-energy band at 595 nm (2.08 eV; likely representing the 0−0 transition) vs that appearing at ∼545 nm (2.27 eV; likely related to the 0−1 transition). Note that the relative intensities of these features are thought to be related to the nature and extent of HJ aggregation in the film for polythiophene-like structures.[61] The presence of an isosbestic point indicates a 1-to-1 species change, further demonstrating the polythiophene species undergo oxidative doping, at least in the voltage range employed here. Upon further increasing the potential to 0.8 V, all three polymers exhibited a small absorption in the visible range, suggesting that the materials can be fully doped within the electrochemical window of water. Each polythiophene in this series exhibited irreversible oxidation at voltages greater than 0.8 V, as evidenced by the simultaneous decrease in the polaronic band and $\pi-\pi^*$ transition (Figure 3d).

P3C(Pr)T, P3C(Bu)T and P3C(Pe)T exhibit similar behavior as highlighted by the impact of voltage on the intensity of bands close to 530 nm (0−1 vibronic band) and 880 nm (polaron formation) (Figure 3e,f). At an applied potential of approximately 0 V for P3C(Bu)T and P3C(Pe)T, and around 0.2 V for P3C(Pr)T, the polymers undergo oxidation. Upon further increases in applied potential, the doping level incrementally increases, as manifested by decay of the 0−1 absorption band and concomitant growth of the polaron band. At a high potential (0.8 V for P3C(Bu)T and P3C(Pe)T, and 0.9 V for P3C(Pr)T), the polaron band increases progressively until reaching a maximum intensity, followed by a decrease. Spectroscopically, the absorbance of neutral and charged features can be utilized to estimate the initial onset potential and facilitate a comparison with the electrochemical characteristics (vide supra). The observed trend aligns with the CV and DPV analysis, where the onset potential for oxidation was found to follow the sequence of P3C(Bu)T ≥ P3C(Pe)T > P3C(Pr)T. Notably, P3C(Bu)T displays a pronounced red shift in both pristine film (Figure S8) and doped/dedoped condition (Figure 3d) relative to the propyl and pentyl alternatives, pointing to stronger intermolecular $\pi-\pi$ polymer backbone stacking and planarization. One potential reason for this disparity lies in the stronger hydrogen bonding interaction induced by P3C(Bu)T.[62] All P3CATs have significant hydrogen bonded C═O vibrational modes, pointing to intermolecular interactions between the polymers. The hydrogen bonded C═O peaks for P3C(Bu)T and P3C(Hex)T (carboxyl-hexyl polythiophene) are shifted to higher energy compared with P3C(Pr)T and P3C(Pe)T by approximately 14 cm^{-1}, indicating stronger hydrogen bonding interactions in the carboxyalkyl chains of these polymers.[62] This phenomenon may also be attributed to changes in molecular packing induced by odd−even effects associated with alkyl chain length, a topic that is currently underexplored in the organic semiconductor field.[63]

Ex situ and in situ Raman spectroscopy enabled further investigation of the neutral polymers upon electrochemical doping and polaron formation and how electrochemical interactions impact OECT performance and stability. An excitation wavelength of 633 nm was selected as a near nonresonant condition to enable simultaneous interrogation of both neutral and oxidized species.[64−66] Figure S9 presents normalized ex situ Raman spectra of P3C(Pr)T, P3C(Bu)T, P3C(Pe)T, and P3HT thin films under ambient condition. Owing to the structural similarities, P3HT was used as a reference for peak assignments. Multiple vibrational modes can be assigned at 600−1600 cm^{-1} for P3HT (Table S4):[67−69] the antisymmetric C═C stretching mode at 1510 cm^{-1}, the symmetric C═C stretching mode at ∼1445 cm^{-1}, C−C intra-ring stretching at ∼1380 cm^{-1}, the C−C inter-ring stretching mode at ∼1209 cm^{-1}, the C−H bending/C−C inter-ring stretching mode at ∼1180 cm^{-1}, the C−C alkyl stretching mode at ∼997 cm^{-1}, and the C−S−C deformation mode at ∼727 cm^{-1}. Here, emphasis will be placed on the two primary in-plane skeleton modes at ∼1445 and ∼1380 cm^{-1} owing to their sensitivity to pi-electron delocalization, electron−phonon coupling, and polaron formation.[68]

The P3CAT spectra resembled P3HT, however two minor differences were observed: (i) the C−C alkyl stretching mode (∼997 cm^{-1} in P3HT) shifted toward to a higher wavenumber (∼1020 cm^{-1} in all P3CATs), presumably due to the incorporation of a carboxylic acid group and the influence of alkyl chain length, and (ii) all carboxylic acid functional polythiophenes exhibit a varying degree of a broad shoulder ranging from 1320 to 1350 cm^{-1} in their pristine forms. The presence of similar features have been observed in oxidized and *p*-doped substituted polythiophenes, attributed to the relatively

https://doi.org/10.1021/acs.chemmater.3c02103
Chem. Mater. 2023, 35, 9299−9312

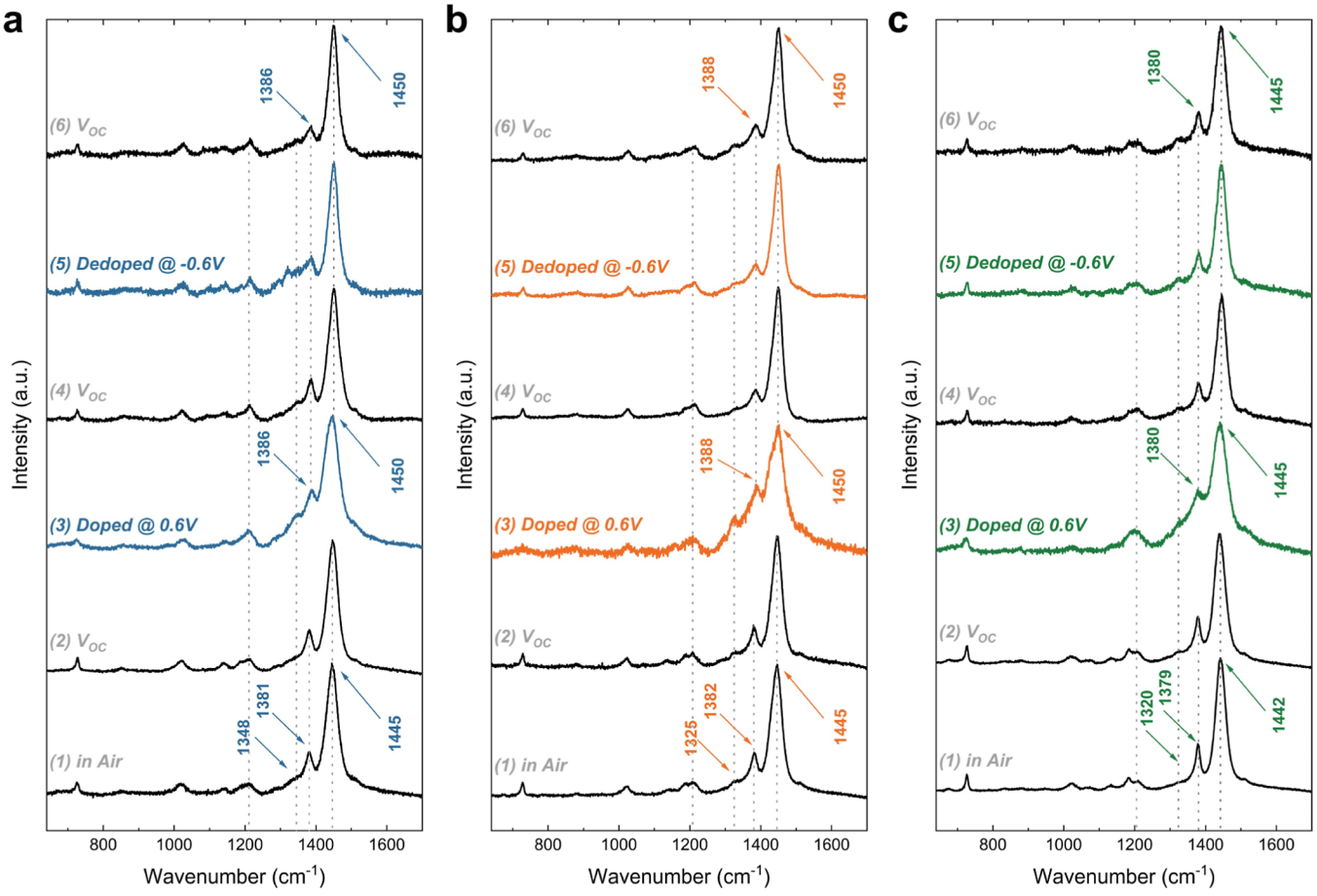

Figure 4. In situ Raman spectrum of (a) P3C(Pr)T (blue), (b) P3C(Bu)T (orange), and (c) P3C(Pe)T (green) performing in 0.1 M NaCl (aq) at an electrochemical cell. The spectra were recorded when the film was (1) dry in air, (2) immersed in electrolyte, (3) doped at 0.6 V vs V_{oc}, (4) subsequently reversed back to V_{oc}, (5) dedoped at −0.6 V vs V_{oc}, and (6) finally reversed back to V_{oc}.

lower degree of molecular order or distorted backbone for P3CATs.[67,69,70] The full width at half-maximum (fwhm) of the C═C mode as well as the relative peak intensity of the two primary in-plane ring skeleton modes ($I_{c-c}/I_{c=c}$) were calculated to compare the degree of molecular order within the P3CAT family. In contrast to P3HT (fwhm = ∼28 cm^{-1}), a much broader peak was observed for P3C(Pr)T (∼38 cm^{-1}), P3C(Bu)T (∼36 cm^{-1}), and P3C(Pe)T (33 cm^{-1}) (Figure S10). Additionally, a lower $I_{c-c}/I_{c=c}$ ratio was apparent for P3C(Pr)T (∼0.111), P3C(Bu)T (∼0.119), and P3C(Pe)T (∼0.123) relative to P3HT (∼0.148). These results indicate that the P3CATs exhibit a reduced level of self-assembly and crystalline features likely attributed to additional steric and interchain interactions resulting from the presence of the terminal carboxylic acid moiety compared to fully alkylated P3HT.[62] Notably, there is a trend of decreased FWHM values and increased $I_{c-c}/I_{c=c}$ ratio as the alkyl length increases from propyl to pentyl, suggesting an enhancement in molecular order.

In situ Raman studies enabled an investigation of the effect of doping/dedoping on the bulk properties of the P3CATs. As shown in Figure 4, the spectral regions for all polymers corresponding to the thiophene ring were unaffected upon exposure to aqueous electrolyte (steps 1 and 2; see Figure S11 for additional details). In contrast, doping at 0.6 V vs V_{oc} (step 3) induced significant changes; namely, a sharper and broader primary in-plane skeleton vibration with a slight shift to higher wavenumber was observed for all three polymers. These changes can be attributed to the proximity of anions to the thiophene backbone and subsequent formation of polarons, leading to a change in hole concentration and substantial quinoid distortion.[71] Doping also enhanced the inter-ring C−C stretching mode at 1180 and 1209 cm^{-1}, indicating a reduction in the overall bond order within the polymer backbone. These effects are commonly observed as a result of charge redistribution, leading to a quinoid-type configuration in polythiophenes.[72] Upon reversing the potential to V_{oc} (step 4), partial recovery of the doping-induced changes along the backbone was observed. Dedoping the polymers at −0.6 V vs V_{oc} (step 5), led to significant distortion near ∼1350 cm^{-1} for P3C(Pr)T, which did not occur in the longer alkyl chain alternatives. Conceivably, P3C(Pr)T may experience more disruption of its packing structure when interacting with water or ions, likely due to its hydrophilicity leading to increased hydration. Finally, when the potential was reversed to V_{oc} (step 6), the longer side chain polymers (P3C(Bu)T, P3C(Pe)T) appeared fully reversible. Overall, the longer alkyl chain polymers, especially P3C(Pe)T, appear to exhibit better retention of their molecular conformation (Figure S12). The observed trend is also aligned with the passive swelling results. Thus, we postulate that the longer alkyl chain polymer more favorably adopts dense solid-state packing, with more rigid bulk properties, rendering a hydrophobic region less capable of coordinating/solvating the ionic and water species and

https://doi.org/10.1021/acs.chemmater.3c02103
Chem. Mater. 2023, 35, 9299−9312

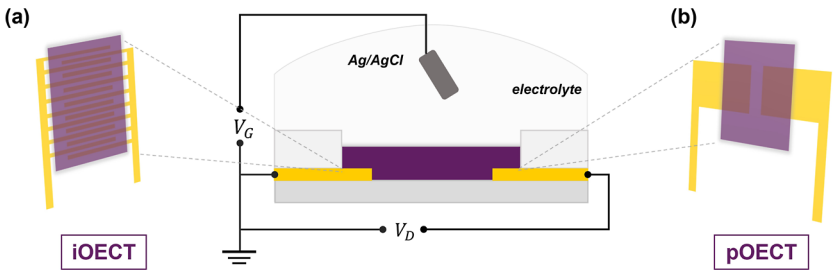

Figure 5. Schematic representations of (a) interdigitated OECT (left) and (b) planar OECT (right) devices using a 0.1 M NaCl (aq) electrolyte.

Table 1. Steady-State OECT Performance Summary for iOECTs and pOECTs

polymer	$g_{m,iOECT}$ [mS][a]	$g_{m,pOECT}$ [S cm^{-1}][b,c]	μC^* [F cm^{-1} V^{-1} s^{-1}][d]	C^* [F cm^{-3}][e]	μ_{OECT} [cm^2 V^{-1} s^{-1}][f]	ON/OFF$_{pOECT}$[c]	ON/OFF$_{iOECT}$[a]
P3C(Pr)T	158 ± 5	35 ± 9	83 ± 3	145 18	0.57 ± 0.06	3.7 × 10^5	2.2 × 10^4
P3C(Bu)T	159 ± 0.5	47 ± 16	107 ± 4	111 ± 14	0.96 ± 0.08	5.3 × 10^4	9.5 × 10^3
P3C(Pe)T	149 ± 2	16 ± 5	38 ± 3	30 ± 5	1.26 ± 0.2	2.6 × 10^4	6.6 × 10^3

[a]Average values calculated across at least three iOECT devices. [b]Normalized transconductance $g_{m,pOECT}$ is calculated according to $g_{m,pOECT} = \frac{L}{Wd} \cdot g_m$. [c]Average values were calculated from at least ten operational channels. [d]μC^* is extracted by linear approximation of transconductance g_m versus channel geometry $\frac{Wd}{L} \cdot (V_{th} - V_g)$, as shown in Figure S14. [e]Extracted from the electrochemical impedance spectra. [f]Mobility values μ are calculated from the μC^* and the volumetric capacitance C^*.

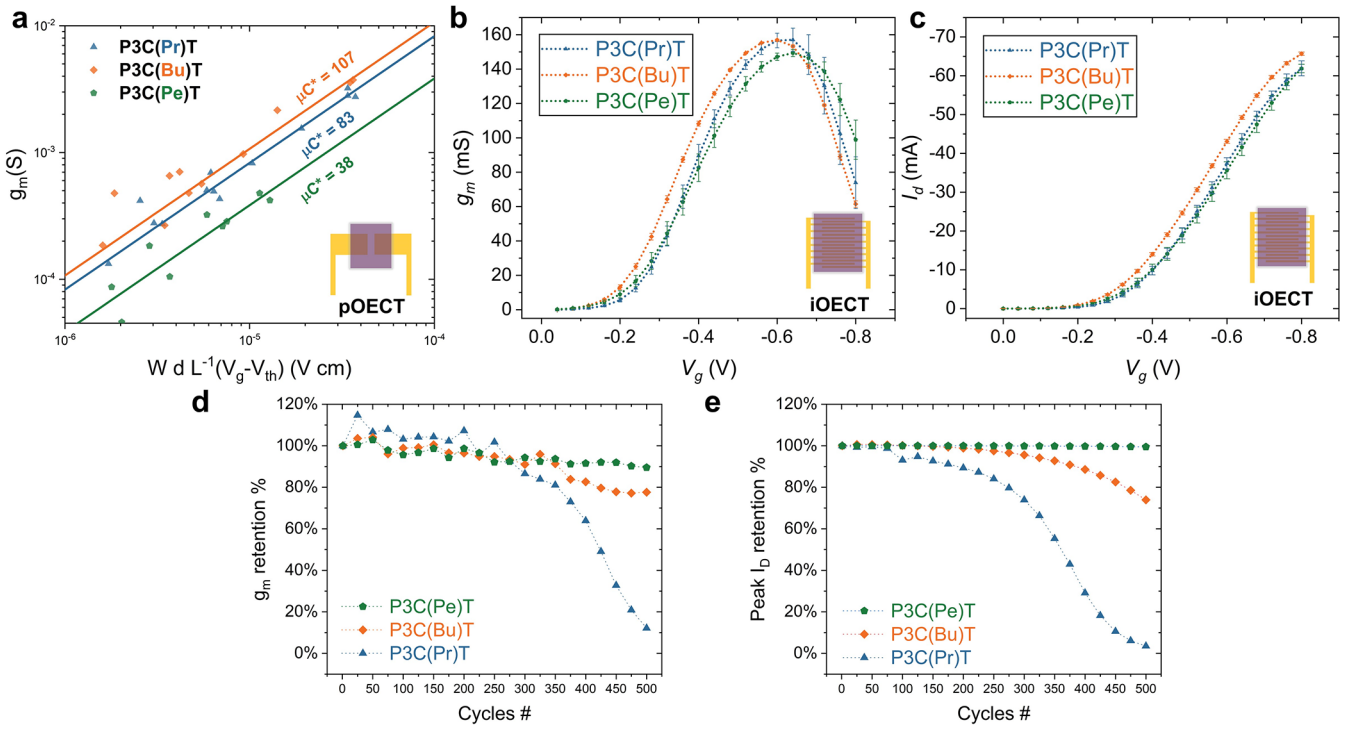

Figure 6. (a) $[\mu C^*]_{pOECT}$ for P3C(Pr)T (blue), P3C(Bu)T (orange), and P3C(Pe)T (green) in pOECT; (b,c) transfer curve and peak current for best performance transconductance for P3C(Pr)T (blue), P3C(Bu)T (orange), and P3C(Pe)T (green) in iOECTs; (d) device stability test for 500 cycle for g_m retention rate; and (e) peak drain current retention rate in iOECTs. The drain voltage is kept at −0.6 V for all measurements.

reducing overall absorption, which is the opposite of the glycolated systems. Consequently, better reversibility as well as enhanced retention of molecular conformation were attained, which, in turn, led to superior stability (vide infra).

OECT Characteristics and Evaluation. To access the mixed conduction behavior of P3C(Pr)T, P3C(Bu)T, and P3C(Pe)T in aqueous media, the materials were incorporated into the OECT devices with different dimensions and geometric configurations (planar OECTs, denoted as pOECTs; and interdigitated OECTs, denoted as iOECTs) (Figure 5). The pOECTs having multiple channel dimensions were used first to evaluate the impact of width/length ratio on transistor performance. All P3CAT-based transistors exhibit p-type accumulation mode operation and display reversible transfer characteristics, as summarized in Table 1 and Figure S13. Maximum transconductance was observed at a gate source voltage of approximately −0.7 V and a threshold voltage $V_{th} \leq -0.33$ V. The ON/OFF ratios were ∼4 × 10^5 for P3C(Pr)T, ∼5 × 10^4 for P3C(Bu)T and ∼3 × 10^4 for P3C(Pe)T, demonstrating the potential for significant signal

https://doi.org/10.1021/acs.chemmater.3c02103
Chem. Mater. 2023, 35, 9299−9312

amplification in bioelectronics applications for this class of OMIEC.

A linear fit for transconductance (g_m) plotted against the various device geometries and operating parameters (Figures 6a and S14) allowed the accurate determination of $[\mu C^*]_{pOECT}$. This assessment of OECT steady-state performance centers around the transconductance (g_m), which denotes the ability of the device to transduce gate voltage (V_g) input into corresponding drain current output (I_d). As expressed in eq 2,[73] Bernard's model provides an effective approximation to correlate transconductance (g_m) with various measured parameters such as threshold voltage (V_{th}), applied gate voltage (V_g), and OECT device geometry including channel width (W), length (L), and thickness (d). The product of OECT mobility and volumetric capacitance, μC^*, provides a figure of merit to benchmark the carboxylated polythiophene family and allows direct comparison with other OMIECs.[21]

$$g_m = \frac{\partial I_d}{\partial V_g} = \frac{Wd}{L} \cdot \mu C^* (V_{th} - V_g) \quad (2)$$

In 0.1 M NaCl (aq) electrolyte, the average $[\mu C^*]_{pOECT}$ values for P3C(Pr)T, P3C(Bu)T, and P3C(Pe)T were 83 ± 3, 107 ± 4, and 38 ± 3 F cm^{-1} V^{-1} s^{-1}, respectively, with the error representing a value equivalent to one standard deviation. Notably, P3C(Bu)T exhibited the highest reported $[\mu C^*]_{pOECT}$ value compared to all reported conjugated polyelectrolytes to date.[74] Representative polymer comparisons from the literature are presented in Table S5. A similar trend for thickness-normalized peak transconductance $g_{m,pOECT}$ was observed, with average values for P3C(Pr)T, P3C(Bu)T and P3C(Pe)T of 35 ± 9, 47 ± 16, and 16 ± 5 S cm^{-1}, respectively. Both polymers functionalized with shorter alkyl spacers show higher transconductance compared to P3C(Pe)T, with the highest value reached by the polymer with butyl spacers, in agreement with the $[\mu C^*]_{pOECT}$ results. The hole mobility, μ_{OECT}, can be further calculated through decoupling $[\mu C^*]_{pOECT}$ with individually measured C^* from EIS. The hole mobility of P3C(Pr)T, P3C(Bu)T and P3C(Pe)T exhibit a monotonic increase with increasing carbon number on the side chain, with 0.57 ± 0.06, 0.96 ± 0.08 and 1.26 ± 0.2 cm^2 V^{-1} s^{-1}, respectively. Notably, these inferred values are relatively high, even when compared to the alkylated counterparts. As a caveat, the accurate μ_{OECT} calculation should be derived through measuring electron/hole transit time from a time or frequency domain and the results obtained here should not be directly compared to mobilities extracted from OFET measurements.[73,75] Likely, the apparent "inflated" value may arise from the effective μ_{OECT} being a measurement of the combination of both ion and hole mobility. Moreover, mobility differences may also be ascribed to the variation in work function across distinct device configurations, ion−polymer interfaces, and polymer processing factors.

To study microstructural effects on the observed improved hole mobility, grazing-incidence wide-angle X-ray scattering (GIWAXS) was performed on the spraycast films. P3C(Pr)T GIWAXS data (Figure S15) demonstrate an isotropic feature with edge-on texture, with lamellar spacing (1.25 nm) and $\pi-\pi$ stacking (0.37 nm) behavior similar to the longer alkyl analogue poly(3-butylthiophene) and P3K(Bu)T.[76,77] Accordingly, the relatively minor change of alkyl length from propyl to butyl and pentyl slightly expands interpolymer side-chain spacing from 1.25 to 1.53 and 1.61 nm, respectively, while the π-spacing remain unchanged (Figure S16). The observed spacing of P3CATs closely aligns with those of poly(3-alkylthiophenes) as determined through GIWAXS analysis.,[76−79] suggesting a similar interlayer structural ordering between P3CATs and P3ATs from a crystalline attribute. Furthermore, within this polymer series, longer alkyl chains are apparently favorable in molecular packing, where the enhanced crystallinity and relatively lower swelling behavior of P3C(Bu)T and P3C(Pe)T support the notion of better preservation of electronic conducting pathways across crystalline and amorphous domains upon exposure to an aqueous environment, rendering superior charge carrier mobility.

The transistor characteristics were next investigated by using an interdigitated contact to explore the performance ceiling of the carboxylated polythiophenes and comprehend device scaling metrics. Relative to the simple rectangular channel geometries, the use of comb-like interdigitated "fingers" in iOECTs is a successful strategy to facilitate the ON current with improved signal amplification owing to the high effective width-to-length (W/L) ratio.[80] As shown in Figures 6b,c and S17−S19, iOECT devices fabricated with comparable thicknesses (90 to 100 nm) of P3C(Pr)T, P3C(Bu)T, and P3C(Pe)T show high $I_{d,max}$, with average values of 62 ± 2, 66 ± 0.4, and 62 ± 1 mA, respectively. These values are accompanied by increased transconductance, where the average peaks $g_{m,iOECT}$ were 158 ± 5, 159 ± 0.5, and 149 ± 2 mS, respectively. Among the three analogs, P3C(Bu)T exhibited the highest drain current and peak transconductance, in agreement with pOECT and electrochemical characterization results.

In comparison to pOECTs, the interdigitated contact provides for a high ON/OFF ratio but with approximately an order of magnitude reduction (Table 1) attributed to the device configuration. These results highlight the potential of iOECTs compared to other geometries to provide outstanding transconductance with advantages such as a reduction in film thickness and active area.[81] This feature holds particular significance in bioelectronics applications, enabling remarkably precise signal capture especially in neuron recording and cellular action potentials, where minimizing device area is essential to accurately record signals with reduced invasiveness.[82,83] However, extensive studies have revealed that there is no linear relationship between transconductance and Wd/L ratio in interdigitated configuration as depicted in eq 2;[83] Consequently, the transconductance of iOECTs does not exhibit a significant increase with an increase in the geometric scaling.[80,84] This observed behavior can be attributed to the dominant influence of contact resistance at the interface between the polymer and electrode.[83,85] Thus, it is essential to thoroughly quantify any material-dependent and device/setup parameters in both planar and interdigitated devices while reporting results, highlighting the importance of a comprehensive understanding of device characteristics and metrics.

In addition to device performance, cycling operational stability is a critical performance metric that must be measured to determine the suitability of candidate materials for practical, long-term OECT applications.[86] Owing to their enhanced sensitivity and application-oriented configuration, iOECTs were chosen to evaluate the stability of P3C(Pr)T, P3C(Bu)T, and P3C(Pe)T during repeated electrochemical cycling. Details of the analysis are provided in the Experimental Section. As presented in Figure 6d, all samples exhibited an

https://doi.org/10.1021/acs.chemmater.3c02103
Chem. Mater. 2023, 35, 9299−9312

initial upward trend for peak g_m while the peak ON current remained relatively stable. After 300 cycles, the P3C(Pr)T peak g_m and ON current began to decrease dramatically, retaining only approximately 10% of its initial g_m and 1% of its initial peak ON current after reaching 500 cycles. P3C(Bu)T and P3C(Pe)T exhibited the best retention rates, maintaining approximately 80 and 90% of their initial transconductance, respectively. Remarkably, P3C(Pe)T retained almost 100% of ON current over the 2 h operation period, while P3C(Bu)T maintained approximately 70% peak ON current, both demonstrating superior stability. Conceivably, the decreased propensity of the Bu and Pe analogs to undergo swelling during cycling in the aqueous electrolyte leads to increased operational stability, in agreement with the in situ Raman results demonstrating that longer alkyl spacer length may enhance conformational rigidity, leading to exceptional stability. We note that the peak current retention rate is not necessarily aligned with the g_m retention rate (Figure 6e), and thus highlight the significance of identifying peak g_m retention as a more application-oriented approach to stability testing, in addition to relying on pulsing measurements.

CONCLUSIONS

In this study, three carboxylated polythiophenes functionalized with alkyl spacers ranging from propyl to pentyl were used to investigate the effect of the carboxylic acid functionality as well as the alkyl spacer length on the OECT performance. The P3KAT precursors were readily spray-cast from water followed by a simple postdeposition acidification step, conferring the material with exceptional resistance to dissolution in common solvents (with the exception of DMSO/NMP/aqueous bases) and/or delamination. Such aqueous processability is crucial for large-scale printed electronics and industrial scaleup, where a preference for benign solvents helps address health, environmental, and financial concerns. The CV and spectroelectrochemical results demonstrate that each of the derivatives can undergo repeated oxidation−reduction cycling in water, pointing to the viability of the P3CAT platform for use as a channel material in OECTs. QCM-D and EIS measurements revealed that −COOH functionalization provides exceptional intrinsic low-swelling behavior as well as substantial charge storage capability. Among the three analogs studied here, P3C(Bu)T passed the highest amount of charge over multiple doping/dedoping cycles. Both decreasing and increasing the alkyl spacer from this optimal length proved detrimental, indicating that a careful "Goldilocks" balance in the alkyl length must be attained in the design of carboxyl-alkyl functionalized conjugated polyelectrolytes for OECTs to maximize their mixed conductivity. In addition, in situ Raman analysis of the polymers was performed. Relative to the propyl derivative, P3C(Bu)T and P3C(Pe)T displayed preferential microstructure with a higher degree of molecular ordering, inducing a favorable rigid bulk conformation toward better operational stability.

Finally, the OECTs were fabricated and evaluated in both planar and interdigitated form factors. Notably, P3C(Bu)T displayed the highest OECT performance in both device configurations, and record-high $[\mu C^*]_{pOECT}$ in the conjugated polyelectrolyte field, indicating a more optimal balance between swelling-enhanced ion dynamics and charge carrier transport. By adapting carboxyl-alkyl functionalization as a solubility enhancer and swelling modifier, our findings demonstrate that this side chain engineering strategy endows the polymer with robust processability and controllable volumetric charge storage without compromising mixed conduction behavior. Thus, the P3CAT platform affords model systems that can facilitate systematic elucidation of the relevant structure/property relationships required for the design of robust OMIECs. The carboxylated side chain functionality, with its commercial viability, ease of (bio)-chemical functionalization, high synthetic flexibility, and aqueous processability, expands the design toolbox and side chain diversity applicable to OMIECs and is expected to pave a new path for tailoring existing p- and n-channel backbones, leading to future highly competitive and biocompatible OMIECs.

ASSOCIATED CONTENT

Supporting Information

The Supporting Information is available free of charge at https://pubs.acs.org/doi/10.1021/acs.chemmater.3c02103.

Differential pulse voltammetry (DPV) onsets, scan-dependent cyclic voltammograms, schematic of electrical impedance spectroscopy (EIS), quartz crystal microbalance with dissipation energy (QCM-D) for swelling measurements, contact angle measurements, UV−vis and spectroelectrochemistry plots, ex situ and in situ Raman spectra, pOECT and iOECT measurement, tabulated comparison for passive swelling and device performance, and GIWAXS spectra (Cartesian plots, chi plots, and in-plane/out-of-plane linecuts) (PDF)

AUTHOR INFORMATION

Corresponding Author

Elsa Reichmanis − *Department of Chemical and Biomolecular Engineering, Lehigh University, Bethlehem, Pennsylvania 18015, United States;* orcid.org/0000-0002-8205-8016; Email: elr420@lehigh.edu

Authors

Zeyuan Sun − *Department of Chemical and Biomolecular Engineering, Lehigh University, Bethlehem, Pennsylvania 18015, United States;* orcid.org/0000-0003-0045-2392

Brian Khau − *School of Chemical and Biomolecular Engineering, Georgia Institute of Technology, Atlanta, Georgia 30332, United States;* Present Address: Pritzker School of Molecular Engineering, University of Chicago, Chicago, Illinois, 60637, United States; Materials Science Division, Argonne National Laboratory, Lemont, Illinois, 60439, United States; orcid.org/0000-0003-4971-8366

Hao Dong − *Department of Chemical and Biomolecular Engineering, Lehigh University, Bethlehem, Pennsylvania 18015, United States;* orcid.org/0000-0002-7383-9523

Christopher J. Takacs − *Stanford Synchrotron Radiation Lightsource SLAC National Accelerator Laboratory, Menlo Park, California 94025, United States*

Shuhan Yuan − *Department of Applied Health Science, School of Public Health, Indiana University, Bloomington, Indiana 47405, United States;* orcid.org/0009-0008-2381-4935

Mengting Sun − *Department of Chemical and Biomolecular Engineering, Lehigh University, Bethlehem, Pennsylvania 18015, United States;* orcid.org/0000-0002-8659-4131

Bar Mosevitzky Lis − *Department of Chemical and Biomolecular Engineering, Lehigh University, Bethlehem,*

https://doi.org/10.1021/acs.chemmater.3c02103
Chem. Mater. 2023, 35, 9299−9312

Pennsylvania 18015, United States; orcid.org/0000-0001-5793-5358

Dang Nguyen − *Department of Chemical and Biomolecular Engineering, Lehigh University, Bethlehem, Pennsylvania 18015, United States;* orcid.org/0009-0005-2959-4820

Complete contact information is available at: https://pubs.acs.org/10.1021/acs.chemmater.3c02103

Author Contributions

The manuscript was written through contributions of all authors. All authors have given approval to the final version of the manuscript.

Notes

The authors declare no competing financial interest.

■ ACKNOWLEDGMENTS

The authors would like to acknowledge support from Lehigh University, funds associated with the Carl Robert Anderson Chair in Chemical Engineering, and device fabrication and characterization facilities associated with the Lehigh University Institute for Functional Materials and Devices. In addition, E.R. and B.K. appreciate partial support from the National Science Foundation grant no. 1809495: Interplay of Molecular Structure and Solution Behavior in High Performance Conjugated Polymers. This work was performed in part at the Georgia Tech Institute for Electronics and Nanotechnology, a member of the National Nanotechnology Coordinated Infrastructure, which is supported by the National Science Foundation (ECCS-1542174). Use of the Stanford Synchrotron Radiation Lightsource, SLAC National Accelerator Laboratory, is supported by the U.S. Department of Energy, Office of Science, Office of Basic Energy Sciences under contract no. DE-AC02-76SF00515. The authors thank Dr. Nathan Wittenberg, Alexandria Pellett, and Dane Santa for assistance with QCM-D measurement.

■ REFERENCES

(1) Paulsen, B. D.; Tybrandt, K.; Stavrinidou, E.; Rivnay, J. Organic Mixed Ionic-Electronic Conductors. *Nat. Mater.* **2020**, *19*, 13−26.

(2) Liang, Y.; Tao, Z.; Chen, J. Organic Electrode Materials for Rechargeable Lithium Batteries. *Adv. Energy Mater.* **2012**, *2* (7), 742−769.

(3) Das, P.; Elizalde-Segovia, R.; Zayat, B.; Salamat, C. Z.; Pace, G.; Zhai, K.; Vincent, R. C.; Dunn, B. S.; Segalman, R. A.; Tolbert, S. H.; Narayan, S. R.; Thompson, B. C. Enhancing the Ionic Conductivity of Poly(3,4-Propylenedioxythiophenes) with Oligoether Side Chains for Use as Conductive Cathode Binders in Lithium-Ion Batteries. *Chem. Mater.* **2022**, *34* (6), 2672−2686.

(4) Gueon, D.; Gonzalez, M. A.; Takeuchi, K. J.; Takeuchi, E. S.; Marschilok, A. C.; Reichmanis, E. Understanding Interfacial Chemistry Interactions in Energy-Dense Lithium-Ion Electrodes. *Acc. Mater. Res.* **2023**, *4* (2), 156−167.

(5) Wang, Y.; Chen, F.; Liu, Z.; Tang, Z.; Yang, Q.; Zhao, Y.; Du, S.; Chen, Q.; Zhi, C. A Highly Elastic and Reversibly Stretchable All-Polymer Supercapacitor. *Angew. Chem., Int. Ed.* **2019**, *58* (44), 15707−15711.

(6) Snook, G. A.; Kao, P.; Best, A. S. Conducting-Polymer-Based Supercapacitor Devices and Electrodes. *J. Power Sources* **2011**, *196* (1), 1−12.

(7) Beaujuge, P. M.; Reynolds, J. R. Color Control in π-Conjugated Organic Polymers for Use in Electrochromic Devices. *Chem. Rev.* **2010**, *110* (1), 268−320.

(8) Deng, Z.; Wang, W.; Xu, X.; Gould, O. E. C.; Kratz, K.; Ma, N.; Lendlein, A. Polymeric Sheet Actuators with Programmable Bioinstructivity. *Proc. Natl. Acad. Sci. U.S.A.* **2020**, *117* (4), 1895−1901.

(9) Malliaras, G.; McCulloch, I. Introduction: Organic Bioelectronics. *Chem. Rev.* **2022**, *122* (4), 4323−4324.

(10) Simon, D. T.; Gabrielsson, E. O.; Tybrandt, K.; Berggren, M. Organic Bioelectronics: Bridging the Signaling Gap between Biology and Technology. *Chem. Rev.* **2016**, *116* (21), 13009−13041.

(11) Rivnay, J.; Owens, R. M.; Malliaras, G. G. The Rise of Organic Bioelectronics. *Chem. Mater.* **2014**, *26* (1), 679−685.

(12) Isaksson, J.; Kjäll, P.; Nilsson, D.; Robinson, N.; Berggren, M.; Richter-Dahlfors, A. Electronic Control of Ca2+ Signalling in Neuronal Cells Using an Organic Electronic Ion Pump. *Nat. Mater.* **2007**, *6* (9), 673−679.

(13) Lee, Y.; Lee, T.-W. Organic Synapses for Neuromorphic Electronics: From Brain-Inspired Computing to Sensorimotor Nervetronics. *Acc. Chem. Res.* **2019**, *52* (4), 964−974.

(14) Zhong, Y.; Saleh, A.; Inal, S. Decoding Electrophysiological Signals with Organic Electrochemical Transistors. *Macromol. Biosci.* **2021**, *21* (11), 2100187.

(15) Rivnay, J.; Inal, S.; Salleo, A.; Owens, R. M.; Berggren, M.; Malliaras, G. G. Organic Electrochemical Transistors. *Nat. Rev. Mater.* **2018**, *3* (2), 17086.

(16) Khau, B. V.; Scholz, A. D.; Reichmanis, E. Advances and Opportunities in Development of Deformable Organic Electrochemical Transistors. *J. Mater. Chem. C* **2020**, *8*, 15067−15078.

(17) Kukhta, N. A.; Marks, A.; Luscombe, C. K. Molecular Design Strategies toward Improvement of Charge Injection and Ionic Conduction in Organic Mixed Ionic-Electronic Conductors for Organic Electrochemical Transistors. *Chem. Rev.* **2022**, *122* (4), 4325−4355.

(18) Inal, S.; Rivnay, J.; Leleux, P.; Ferro, M.; Ramuz, M.; Brendel, J. C.; Schmidt, M. M.; Thelakkat, M.; Malliaras, G. G.; Inal, S.; Rivnay, J.; Leleux, P.; Ferro, M.; Ramuz, M.; Malliaras, G. G.; Brendel, J. C.; Schmidt, M. M.; Thelakkat, M. A High Transconductance Accumulation Mode Electrochemical Transistor. *Adv. Mater.* **2014**, *26* (44), 7450−7455.

(19) Rivnay, J.; Inal, S.; Collins, B. A.; Sessolo, M.; Stavrinidou, E.; Strakosas, X.; Tassone, C.; Delongchamp, D. M.; Malliaras, G. G. Structural Control of Mixed Ionic and Electronic Transport in Conducting Polymers. *Nat. Commun.* **2016**, *7* (1), 11287.

(20) Nielsen, C. B.; Giovannitti, A.; Sbircea, D. T.; Bandiello, E.; Niazi, M. R.; Hanifi, D. A.; Sessolo, M.; Amassian, A.; Malliaras, G. G.; Rivnay, J.; McCulloch, I. Molecular Design of Semiconducting Polymers for High-Performance Organic Electrochemical Transistors. *J. Am. Chem. Soc.* **2016**, *138* (32), 10252−10259.

(21) Inal, S.; Malliaras, G. G.; Rivnay, J. Benchmarking Organic Mixed Conductors for Transistors. *Nat. Commun.* **2017**, *8* (1), 1767.

(22) Kim, S.-M.; Kim, C.-H.; Kim, Y.; Kim, N.; Lee, W.-J.; Lee, E.-H.; Kim, D.; Park, S.; Lee, K.; Rivnay, J.; Yoon, M.-H. Influence of PEDOT:PSS Crystallinity and Composition on Electrochemical Transistor Performance and Long-Term Stability. *Nat. Commun.* **2018**, *9* (1), 3858.

(23) ElMahmoudy, M.; Inal, S.; Charrier, A.; Uguz, I.; Malliaras, G. G.; Sanaur, S. Tailoring the Electrochemical and Mechanical Properties of PEDOT:PSS Films for Bioelectronics. *Macromol. Mater. Eng.* **2017**, *302* (5), 1600497.

(24) Mei, J.; Bao, Z. Side Chain Engineering in Solution-Processable Conjugated Polymers. *Chem. Mater.* **2014**, *26* (1), 604−615.

(25) Savagian, L. R.; Österholm, A. M.; Ponder, J. F.; Barth, K. J.; Rivnay, J.; Reynolds, J. R. Balancing Charge Storage and Mobility in an Oligo(Ether) Functionalized Dioxythiophene Copolymer for Organic- and Aqueous- Based Electrochemical Devices and Transistors. *Adv. Mater.* **2018**, *30* (50), 1804647.

(26) Flagg, L. Q.; Bischak, C. G.; Onorato, J. W.; Rashid, R. B.; Luscombe, C. K.; Ginger, D. S. Polymer Crystallinity Controls Water Uptake in Glycol Side-Chain Polymer Organic Electrochemical Transistors. *J. Am. Chem. Soc.* **2019**, *141* (10), 4345−4354.

(27) Giovannitti, A.; Sbircea, D. T.; Inal, S.; Nielsen, C. B.; Bandiello, E.; Hanifi, D. A.; Sessolo, M.; Malliaras, G. G.; McCulloch,

I.; Rivnay, J. Controlling the Mode of Operation of Organic Transistors through Side-Chain Engineering. *Proc. Natl. Acad. Sci. U.S.A.* **2016**, *113* (43), 12017−12022.
(28) Giovannitti, A.; Nielsen, C. B.; Sbircea, D.-T.; Inal, S.; Donahue, M.; Niazi, M. R.; Hanifi, D. A.; Amassian, A.; Malliaras, G. G.; Rivnay, J.; McCulloch, I. N-Type Organic Electrochemical Transistors with Stability in Water. *Nat. Commun.* **2016**, *7* (1), 13066.
(29) Schmode, P.; Savva, A.; Kahl, R.; Ohayon, D.; Meichsner, F.; Dolynchuk, O.; Thurn-Albrecht, T.; Inal, S.; Thelakkat, M. The Key Role of Side Chain Linkage in Structure Formation and Mixed Conduction of Ethylene Glycol Substituted Polythiophenes. *ACS Appl. Mater. Interfaces* **2020**, *12* (11), 13029−13039.
(30) Nicolini, T.; Surgailis, J.; Savva, A.; Scaccabarozzi, A. D.; Nakar, R.; Thuau, D.; Wantz, G.; Richter, L. J.; Dautel, O.; Hadziioannou, G.; Stingelin, N. A Low-Swelling Polymeric Mixed Conductor Operating in Aqueous Electrolytes. *Adv. Mater.* **2021**, *33* (2), 2005723.
(31) Dyson, M. J.; Lariou, E.; Martin, J.; Li, R.; Erothu, H.; Wantz, G.; Topham, P. D.; Dautel, O. J.; Hayes, S. C.; Stavrinou, P. N.; Stingelin, N. Managing Local Order in Conjugated Polymer Blends via Polarity Contrast. *Chem. Mater.* **2019**, *31* (17), 6540−6547.
(32) Moser, M.; Savagian, L. R.; Savva, A.; Matta, M.; Ponder, J. F.; Hidalgo, T. C.; Ohayon, D.; Hallani, R.; Reisjalali, M.; Troisi, A.; Wadsworth, A.; Reynolds, J. R.; Inal, S.; McCulloch, I. Ethylene Glycol-Based Side Chain Length Engineering in Polythiophenes and Its Impact on Organic Electrochemical Transistor Performance. *Chem. Mater.* **2020**, *32* (15), 6618−6628.
(33) Noriega, R.; Rivnay, J.; Vandewal, K.; Koch, F. P. V.; Stingelin, N.; Smith, P.; Toney, M. F.; Salleo, A. A General Relationship between Disorder, Aggregation and Charge Transport in Conjugated Polymers. *Nat. Mater.* **2013**, *12* (11), 1038−1044.
(34) Maria, I. P.; Paulsen, B. D.; Savva, A.; Ohayon, D.; Wu, R.; Hallani, R.; Basu, A.; Du, W.; Anthopoulos, T. D.; Inal, S.; Rivnay, J.; McCulloch, I.; Giovannitti, A. The Effect of Alkyl Spacers on the Mixed Ionic-Electronic Conduction Properties of N-Type Polymers. *Adv. Funct. Mater.* **2021**, *31* (14), 2008718.
(35) Tan, S. T. M.; Lee, G.; Denti, I.; LeCroy, G.; Rozylowicz, K.; Marks, A.; Griggs, S.; McCulloch, I.; Giovannitti, A.; Salleo, A. Tuning Organic Electrochemical Transistor Threshold Voltage Using Chemically Doped Polymer Gates. *Adv. Mater.* **2022**, *34* (33), 2202359.
(36) Wang, Y.; Zeglio, E.; Liao, H.; Xu, J.; Liu, F.; Li, Z.; Maria, I. P.; Mawad, D.; Herland, A.; McCulloch, I.; Yue, W. Hybrid Alkyl-Ethylene Glycol Side Chains Enhance Substrate Adhesion and Operational Stability in Accumulation Mode Organic Electrochemical Transistors. *Chem. Mater.* **2019**, *31* (23), 9797−9806.
(37) Schmode, P.; Ohayon, D.; Reichstein, P. M.; Savva, A.; Inal, S.; Thelakkat, M. High-Performance Organic Electrochemical Transistors Based on Conjugated Polyelectrolyte Copolymers. *Chem. Mater.* **2019**, *31* (14), 5286−5295.
(38) Zeglio, E.; Eriksson, J.; Gabrielsson, R.; Solin, N.; Inganäs, O. Highly Stable Conjugated Polyelectrolytes for Water-Based Hybrid Mode Electrochemical Transistors. *Adv. Mater.* **2017**, *29* (19), 1605787.
(39) Zeglio, E.; Vagin, M.; Musumeci, C.; Ajjan, F. N.; Gabrielsson, R.; Trinh, X. T.; Son, N. T.; Maziz, A.; Solin, N.; Inganäs, O. Conjugated Polyelectrolyte Blends for Electrochromic and Electrochemical Transistor Devices. *Chem. Mater.* **2015**, *27* (18), 6385−6393.
(40) Nguyen-Dang, T.; Chae, S.; Chatsirisupachai, J.; Wakidi, H.; Promarak, V.; Visell, Y.; Nguyen, T.-Q. Dual-Mode Organic Electrochemical Transistors Based on Self-Doped Conjugated Polyelectrolytes for Reconfigurable Electronics. *Adv. Mater.* **2022**, *34* (23), No. e2200274.
(41) Khau, B. V.; Savagian, L. R.; De Keersmaecker, M.; Gonzalez, M. A.; Reichmanis, E. Carboxylic Acid Functionalization Yields Solvent-Resistant Organic Electrochemical Transistors. *ACS Mater. Lett.* **2019**, *1* (6), 599−605.
(42) Luo, S.-C.; Mohamed Ali, E.; Tansil, N. C.; Yu, H.; Gao, S.; Kantchev, E. A. B.; Ying, J. Y. Poly(3,4-Ethylenedioxythiophene) (PEDOT) Nanobiointerfaces: Thin, Ultrasmooth, and Functionalized PEDOT Films with in Vitro and in Vivo Biocompatibility. *Langmuir* **2008**, *24* (15), 8071−8077.
(43) Povlich, L. K.; Cho, J. C.; Leach, M. K.; Corey, J. M.; Kim, J.; Martin, D. C. Synthesis, Copolymerization and Peptide-Modification of Carboxylic Acid-Functionalized 3,4-Ethylenedioxythiophene (EDOTacid) for Neural Electrode Interfaces. *Biochim. Biophys. Acta* **2013**, *1830* (9), 4288−4293.
(44) Ji, X.; Lin, X.; Rivnay, J. Organic Electrochemical Transistors as On-Site Signal Amplifiers for Electrochemical Aptamer-Based Sensing. *Nat. Commun.* **2023**, *14* (1), 1665.
(45) Mawad, D.; Artzy-Schnirman, A.; Tonkin, J.; Ramos, J.; Inal, S.; Mahat, M. M.; Darwish, N.; Zwi-Dantsis, L.; Malliaras, G. G.; Gooding, J. J.; Lauto, A.; Stevens, M. M. Electroconductive Hydrogel Based on Functional Poly(Ethylenedioxy Thiophene). *Chem. Mater.* **2016**, *28* (17), 6080−6088.
(46) Tan, E.; Kim, J.; Stewart, K.; Pitsalidis, C.; Kwon, S.; Siemons, N.; Kim, J.; Jiang, Y.; Frost, J. M.; Pearce, D.; Tyrrell, J. E.; Nelson, J.; Owens, R. M.; Kim, Y.; Kim, J. The Role of Long-Alkyl-Group Spacers in Glycolated Copolymers for High-Performance Organic Electrochemical Transistors. *Adv. Mater.* **2022**, *34* (27), 2202574.
(47) Kaplin, D. A.; Qutubuddin, S. Electrochemically Synthesized Polypyrrole Films: Effects of Polymerization Potential and Electrolyte Type. *Polymer* **1995**, *36* (6), 1275−1286.
(48) Bard, A. J.; Faulkner, L. R.; White, H. S. *Electrochemical Methods: Fundamentals and Applications*; John Wiley & Sons, 2022.
(49) Lyons, M. E. G. *Electroactive Polymer Electrochemistry*; Lyons, M. E. G., Ed.; Springer US: Boston, MA, 1994..
(50) Tybrandt, K.; Zozoulenko, I. V.; Berggren, M. Chemical Potential-Electric Double Layer Coupling in Conjugated Polymer-Polyelectrolyte Blends. *Sci. Adv.* **2017**, *3* (12), No. eaao3659.
(51) Volkov, A. V.; Wijeratne, K.; Mitraka, E.; Ail, U.; Zhao, D.; Tybrandt, K.; Andreasen, J. W.; Berggren, M.; Crispin, X.; Zozoulenko, I. V. Understanding the Capacitance of PEDOT:PSS. *Adv. Funct. Mater.* **2017**, *27* (28), 1700329.
(52) Ferloni, P.; Mastragostino, M.; Meneghello, L. Impedance Analysis of Electronically Conducting Polymers. *Electrochim. Acta* **1996**, *41* (1), 27−33.
(53) Giovannitti, A.; Maria, I. P.; Hanifi, D.; Donahue, M. J.; Bryant, D.; Barth, K. J.; Makdah, B. E.; Savva, A.; Moia, D.; Zetek, M.; Barnes, P. R. F.; Reid, O. G.; Inal, S.; Rumbles, G.; Malliaras, G. G.; Nelson, J.; Rivnay, J.; McCulloch, I. The Role of the Side Chain on the Performance of N-Type Conjugated Polymers in Aqueous Electrolytes. *Chem. Mater.* **2018**, *30* (9), 2945−2953.
(54) Savva, A.; Hallani, R.; Cendra, C.; Surgailis, J.; Hidalgo, T. C.; Wustoni, S.; Sheelamanthula, R.; Chen, X.; Kirkus, M.; Giovannitti, A.; Salleo, A.; McCulloch, I.; Inal, S. Balancing Ionic and Electronic Conduction for High-Performance Organic Electrochemical Transistors. *Adv. Funct. Mater.* **2020**, *30* (11), 1907657.
(55) Savva, A.; Wustoni, S.; Inal, S. Ionic-to-Electronic Coupling Efficiency in PEDOT:PSS Films Operated in Aqueous Electrolytes. *J. Mater. Chem. C* **2018**, *6* (44), 12023−12030.
(56) Moser, M.; Hidalgo, T. C.; Surgailis, J.; Gladisch, J.; Ghosh, S.; Sheelamanthula, R.; Thiburce, Q.; Giovannitti, A.; Salleo, A.; Gasparini, N.; Wadsworth, A.; Zozoulenko, I.; Berggren, M.; Stavrinidou, E.; Inal, S.; McCulloch, I. Side Chain Redistribution as a Strategy to Boost Organic Electrochemical Transistor Performance and Stability. *Adv. Mater.* **2020**, *32* (37), 2002748.
(57) Savva, A.; Cendra, C.; Giugni, A.; Torre, B.; Surgailis, J.; Ohayon, D.; Giovannitti, A.; McCulloch, I.; Di Fabrizio, E.; Salleo, A.; Rivnay, J.; Inal, S. Influence of Water on the Performance of Organic Electrochemical Transistors. *Chem. Mater.* **2019**, *31* (3), 927−937.
(58) Moia, D.; Giovannitti, A.; Szumska, A. A.; Maria, I. P.; Rezasoltani, E.; Sachs, M.; Schnurr, M.; Barnes, P. R. F.; McCulloch, I.; Nelson, J. Design and Evaluation of Conjugated Polymers with Polar Side Chains as Electrode Materials for Electrochemical Energy Storage in Aqueous Electrolytes. *Energy Environ. Sci.* **2019**, *12* (4), 1349−1357.

https://doi.org/10.1021/acs.chemmater.3c02103
Chem. Mater. 2023, 35, 9299−9312

(59) Stavrinidou, E.; Leleux, P.; Rajaona, H.; Khodagholy, D.; Rivnay, J.; Lindau, M.; Sanaur, S.; Malliaras, G. G. Direct Measurement of Ion Mobility in a Conducting Polymer. *Adv. Mater.* **2013**, *25* (32), 4488−4493.
(60) Inal, S.; Rivnay, J.; Hofmann, A. I.; Uguz, I.; Mumtaz, M.; Katsigiannopoulos, D.; Brochon, C.; Cloutet, E.; Hadziioannou, G.; Malliaras, G. G. Organic Electrochemical Transistors Based on PEDOT with Different Anionic Polyelectrolyte Dopants. *J. Polym. Sci., Part B: Polym. Phys.* **2016**, *54* (2), 147−151.
(61) Spano, F. C.; Silva, C. H- and J-Aggregate Behavior in Polymeric Semiconductors. *Annu. Rev. Phys. Chem.* **2014**, *65* (1), 477−500.
(62) Worfolk, B. J.; Rider, D. A.; Elias, A. L.; Thomas, M.; Harris, K. D.; Buriak, J. M. Bulk Heterojunction Organic Photovoltaics Based on Carboxylated Polythiophenes and PCBM on Glass and Plastic Substrates. *Adv. Funct. Mater.* **2011**, *21* (10), 1816−1826.
(63) Burnett, E. K.; Ai, Q.; Cherniawski, B. P.; Parkin, S. R.; Risko, C.; Briseno, A. L. Even-Odd Alkyl Chain-Length Alternation Regulates Oligothiophene Crystal Structure. *Chem. Mater.* **2019**, *31* (17), 6900−6907.
(64) Shi, G.; Xu, J.; Fu, M. Raman Spectroscopic and Electrochemical Studies on the Doping Level Changes of Polythiophene Films during Their Electrochemical Growth Processes. *J. Phys. Chem. B* **2002**, *106* (2), 288−292.
(65) Louarn, G.; Trznadel, M.; Buisson, J. P.; Laska, J.; Pron, A.; Lapkowski, M.; Lefrant, S. Raman Spectroscopic Studies of Regioregular Poly(3-Alkylthiophenes). *J. Phys. Chem.* **1996**, *100* (30), 12532−12539.
(66) Peng, H.; Zhang, L.; Spires, J.; Soeller, C.; Travas-Sejdic, J. Synthesis of a Functionalized Polythiophene as an Active Substrate for a Label-Free Electrochemical Genosensor. *Polymer* **2007**, *48* (12), 3413−3419.
(67) Mansour, A. E.; Valencia, A. M.; Lungwitz, D.; Wegner, B.; Tanaka, N.; Shoji, Y.; Fukushima, T.; Opitz, A.; Cocchi, C.; Koch, N. Understanding the Evolution of the Raman Spectra of Molecularly P-Doped Poly(3-Hexylthiophene-2,5-Diyl): Signatures of Polarons and Bipolarons. *Phys. Chem. Chem. Phys.* **2022**, *24* (5), 3109−3118.
(68) Tsoi, W. C.; James, D. T.; Kim, J. S.; Nicholson, P. G.; Murphy, C. E.; Bradley, D. D. C.; Nelson, J.; Kim, J. S. The Nature of In-Plane Skeleton Raman Modes of P3HT and Their Correlation to the Degree of Molecular Order in P3HT:PCBM Blend Thin Films. *J. Am. Chem. Soc.* **2011**, *133* (25), 9834−9843.
(69) Baibarac, M.; Lapkowski, M.; Pron, A.; Lefrant, S.; Baltog, I. SERS Spectra of Poly(3-Hexylthiophene) in Oxidized and Unoxidized States. *J. Raman Spectrosc.* **1998**, *29* (9), 825−832.
(70) Yamamoto, J.; Furukawa, Y. Electronic and Vibrational Spectra of Positive Polarons and Bipolarons in Regioregular Poly(3-Hexylthiophene) Doped with Ferric Chloride. *J. Phys. Chem. B* **2015**, *119* (13), 4788−4794.
(71) Keene, S. T.; Pol, T. P. A.; Zakhidov, D.; Weijtens, C. H. L.; Janssen, R. A. J.; Salleo, A.; Burgt, Y. Enhancement-Mode PEDOT:PSS Organic Electrochemical Transistors Using Molecular De-Doping. *Adv. Mater.* **2020**, *32* (19), 2000270.
(72) Milani, A.; Brambilla, L.; Del Zoppo, M.; Zerbi, G. Raman Dispersion and Intermolecular Interactions in Unsubstituted Thiophene Oligomers. *J. Phys. Chem. B* **2007**, *111* (6), 1271−1276.
(73) Bernards, D. A.; Malliaras, G. G. Steady-State and Transient Behavior of Organic Electrochemical Transistors. *Adv. Funct. Mater.* **2007**, *17* (17), 3538−3544.
(74) Li, P.; Lei, T. Molecular Design Strategies for High-performance Organic Electrochemical Transistors. *J. Polym. Sci.* **2022**, *60* (3), 377−392.
(75) Ohayon, D.; Druet, V.; Inal, S. A Guide for the Characterization of Organic Electrochemical Transistors and Channel Materials. *Chem. Soc. Rev.* **2023**, *52* (3), 1001−1023.
(76) Grocke, G. L.; Dong, B. X.; Taggart, A. D.; Martinson, A. B. F.; Niklas, J.; Poluektov, O. G.; Strzalka, J. W.; Patel, S. N. Structure-Transport Properties Governing the Interplay in Humidity-Dependent Mixed Ionic and Electronic Conduction of Conjugated Polyelectrolytes. *ACS Polym. Au* **2022**, *2* (4), 275−286.
(77) Liu, Y.; Xian, K.; Gui, R.; Zhou, K.; Liu, J.; Gao, M.; Zhao, W.; Jiao, X.; Deng, Y.; Yin, H.; Geng, Y.; Ye, L. Simple Polythiophene Solar Cells Approaching 10% Efficiency via Carbon Chain Length Modulation of Poly(3-Alkylthiophene). *Macromolecules* **2022**, *55* (1), 133−145.
(78) Mai, C.-K.; Schlitz, R. A.; Su, G. M.; Spitzer, D.; Wang, X.; Fronk, S. L.; Cahill, D. G.; Chabinyc, M. L.; Bazan, G. C. Side-Chain Effects on the Conductivity, Morphology, and Thermoelectric Properties of Self-Doped Narrow-Band-Gap Conjugated Polyelectrolytes. *J. Am. Chem. Soc.* **2014**, *136* (39), 13478−13481.
(79) Harris, J. K.; Ratcliff, E. L. Ion Diffusion Coefficients in Poly(3-Alkylthiophenes) for Energy Conversion and Biosensing: Role of Side-Chain Length and Microstructure. *J. Mater. Chem. C* **2020**, *8* (38), 13319−13327.
(80) Lill, A. T.; Cao, D. X.; Schrock, M.; Vollbrecht, J.; Huang, J.; Nguyen-Dang, T.; Brus, V. V.; Yurash, B.; Leifert, D.; Bazan, G. C.; Nguyen, T. Organic Electrochemical Transistors Based on the Conjugated Polyelectrolyte PCPDTBT-SO $_3$ K (CPE-K). *Adv. Mater.* **2020**, *32* (33), 1908120.
(81) Tyrrell, J. E.; Boutelle, M. G.; Campbell, A. J. Measurement of Electrophysiological Signals In Vitro Using High-Performance Organic Electrochemical Transistors. *Adv. Funct. Mater.* **2021**, *31* (1), 2007086.
(82) Khodagholy, D.; Doublet, T.; Quilichini, P.; Gurfinkel, M.; Leleux, P.; Ghestem, A.; Ismailova, E.; Hervé, T.; Sanaur, S.; Bernard, C.; Malliaras, G. G. In Vivo Recordings of Brain Activity Using Organic Transistors. *Nat. Commun.* **2013**, *4* (1), 1575.
(83) Liang, Y.; Brings, F.; Maybeck, V.; Ingebrandt, S.; Wolfrum, B.; Pich, A.; Offenhäusser, A.; Mayer, D. Tuning Channel Architecture of Interdigitated Organic Electrochemical Transistors for Recording the Action Potentials of Electrogenic Cells. *Adv. Funct. Mater.* **2019**, *29* (29), 1902085.
(84) DiTullio, B. T.; Savagian, L. R.; Bardagot, O.; De Keersmaecker, M.; Österholm, A. M.; Banerji, N.; Reynolds, J. R. Effects of Side-Chain Length and Functionality on Polar Poly(Dioxythiophene)s for Saline-Based Organic Electrochemical Transistors. *J. Am. Chem. Soc.* **2023**, *145* (1), 122−134.
(85) Kaphle, V.; Liu, S.; Al-Shadeedi, A.; Keum, C.-M.; Lüssem, B. Contact Resistance Effects in Highly Doped Organic Electrochemical Transistors. *Adv. Mater.* **2016**, *28* (39), 8766−8770.
(86) Huang, W.; Chen, J.; Yao, Y.; Zheng, D.; Ji, X.; Feng, L.-W.; Moore, D.; Glavin, N. R.; Xie, M.; Chen, Y.; Pankow, R. M.; Surendran, A.; Wang, Z.; Xia, Y.; Bai, L.; Rivnay, J.; Ping, J.; Guo, X.; Cheng, Y.; Marks, T. J.; Facchetti, A. Vertical Organic Electrochemical Transistors for Complementary Circuits. *Nature* **2023**, *613* (7944), 496−502.

https://doi.org/10.1021/acs.chemmater.3c02103
Chem. Mater. 2023, 35, 9299−9312